Journal of Medicinal Chemistry

Article

Structure-guided Discovery of Novel, Potent and Orally Bioavailable Inhibitors of Lipoprotein-associated Phospholipase A2

Qiufeng Liu, Fubao Huang, Xiao-Jing Yuan, Kai Wang, Yi Zou, Jianhua Shen, and Yechun Xu

J. Med. Chem., **Just Accepted Manuscript** • DOI: 10.1021/acs.jmedchem.7b01530 • Publication Date (Web): 01 Dec 2017

Just Accepted

ACS Publications

Journal of Medicinal Chemistry is published by the American Chemical Society. 1155 Sixteenth Street N.W., Washington, DC 20036

Structure-guided Discovery of Novel, Potent and Orally Bioavailable Inhibitors of Lipoprotein-associated Phospholipase A2

Qiufeng Liu[‖#§‡], Fubao Huang[⊥§‡], Xiaojing Yuan[‖§‡], Kai Wang[⊥], Yi Zou[‖], Jianhua Shen[⊥*], and Yechun Xu[‖*]

[‖]CAS Key Laboratory of Receptor Research, [⊥]State Key Laboratory of Drug Research, Drug Discovery and Design Center, Shanghai Institute of Materia Medica, Chinese Academy of Sciences (CAS), Shanghai 201203, China.

[#]School of Life Science and Technology, ShanghaiTech University, Shanghai 200031, China

[§] University of Chinese Academy of Sciences, Beijing, 100049, China

KEYWORDS Lipoprotein-associated phospholipase A2 Inhibitor, Sulfonamide scaffold, Fragment-based lead discovery, Structure-based hit-to-lead optimization, Pharmacokinetics

ABSTRACT

Lipoprotein-associated phospholipase A2 (Lp-PLA2) is a promising therapeutic target for atherosclerosis, Alzheimer's disease and diabetic macular edema. Here we report the identification of novel sulfonamide scaffold Lp-PLA2 inhibitors derived from a relatively weak fragment. Similarity searching on this fragment followed by molecular docking leads to the discovery of a micromolar inhibitor with 300-fold potency improvement. By the application of a structure-guided design strategy, a successful hit-to-lead optimization was achieved and a number of Lp-PLA2 inhibitors with single-digit nanomolar activity were obtained. After preliminary evaluation of the properties of drug-likeness *in vitro* and *in vivo*, compound **37** outstands from this congeneric series of inhibitors for good inhibitory activity and favorable oral bioavailability in male Sprague-Dawley rats, providing a quality candidate for further development. Our current study thus clearly demonstrates the power and advantage of integrally employing fragment screening, complex crystal structures, virtual screening, and medicinal chemistry in an efficient lead discovery project, providing a good example for structure-based drug design.

INTRODUCTION

Lipoprotein-associated phospholipase A2 (Lp-PLA2) belongs to the phospholipase A2 superfamily.[1] The 3D structure of Lp-PLA2 adopts a canonical lipase α/β-hydrolase conformation and contains a large substrate binding pocket starting from the catalytic triad (Ser273, His351 and Asp296) to lipoprotein binding helices.[2] In human plasma, Lp-PLA2 mainly associates with low density lipoproteins (LDL) and hydrolyzes the sn-2 ester bond in platelet activating factor (PAF)[3] and other recognized phospholipids.[4] Specifically, Lp-PLA2 can hydrolyze oxidized modified phospholipids into several pro-inflammatory stimuli, such as lysophosphatidylcholine (lyso-PC) and oxidized non-esterified free fatty acids (ox-NEFA), both of which trigger a series of inflammatory responses. Both Lp-PLA2 activity and mass have shown recurrent association with risk of coronary heart disease (CHD) in a meta-analysis.[5] And Lp-PLA2 was demonstrated to be an independent biomarker of poor prognosis for coronary artery disease.[6] Selective inhibition of this enzyme showed protective effects on blood-brain barrier (BBB) dysfunction in a pig model.[7] Moreover, Lp-PLA2 was involved in retinal vasopermeability and the pathogenesis of diabetic macular edema (DME).[8] Accordingly, inhibition of Lp-PLA2 may be a potential therapy for clinical intervention on atherosclerosis inflammation, Alzheimer's disease and DME, and a promising approach to address the underlying pathological mechanisms.

Owing to the interest in Lp-PLA2 as a promising therapeutic target, several classes of

Lp-PLA2 inhibitors have been reported (Figure 1).[9] The majority of them occupied the catalytic site of Lp-PLA2, such as lactams (**1**)[10], oximes (**2**)[11], amides of xanthurenic acid (**3**)[12], carbamates (**4**)[13], pyrimidone derivatives (**5** and **7**)[14], or imidazo[1,2-a]pyrimidine derivatives (**6**)[15]. Darapladib (**5**) is the most advanced Lp-PLA2 inhibitor in the clinic, though it failed to meet the primary end points in two phase III clinical trials focusing on coronary heart disease.[16] This raises the concern about Lp-PLA2 if it is a target for development of therapeutic agents or it may just serve as a biomarker of vascular inflammation.[9, 17] However, in a 3-month placebo-controlled study, darapladib showed modest improvement in vision and macular edema in DME patients.[18] In addition, Rilapladib, another Lp-PLA2 inhibitor, is in the phase II clinical trial for the treatment of Alzheimer's disease.[19] Therefore, inhibitors with different scaffolds should be explored to better investigate the clinical intervention on Lp-PLA2.

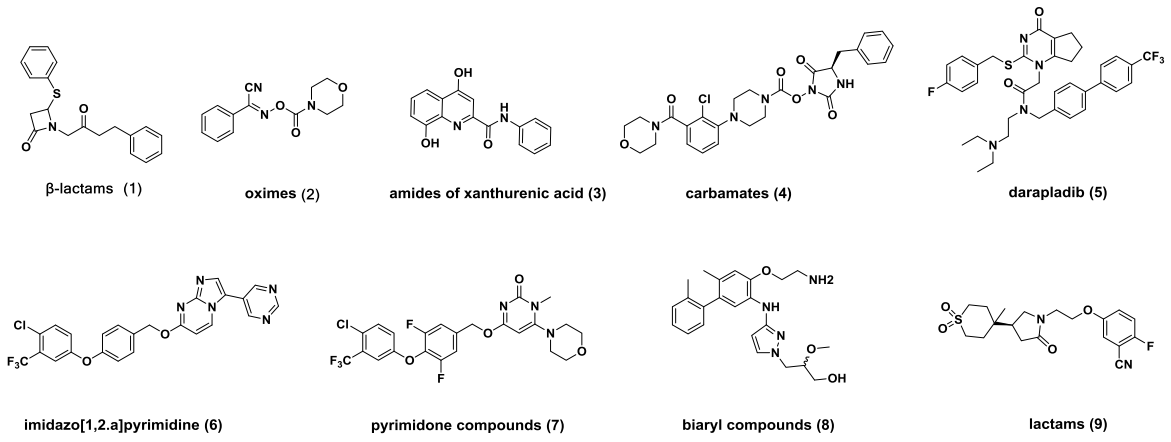

Figure 1. Selected examples of reported Lp-PLA2 inhibitors.

Previously, we have reported imidazo[1,2-a]pyrimidine derivatives as potent and orally bioavailable Lp-PLA2 inhibitors.[15] A further study led to the identification of the

pyrimidone inhibitors, which significantly degraded the retinal thickening in a Sprague-Dawley rat model of DME.[20] We also disclosed the crystal structures of Lp-PLA2 in complex with two inhibitors, darapladib and a pyrimidone derivative, and shed lights on the binding mechanisms of different inhibitors with Lp-PLA2[2b], providing an important prerequisite for the accomplishment of a successful fragment-based lead discovery (FBLD) project. FBLD has matured over the last decade to a reliable and efficient method, and has been generating promising leads for subsequent medicinal chemistry optimization.[21] Recently, Astex together with Glaxosmithkline (GSK) applied the FBLD strategy to identify novel Lp-PLA2 inhibitors (compound **8**[22] and **9**[23]).

Aiming to identify potent Lp-PLA2 inhibitors with new scaffolds, we screened our in-house 500-fragment library with the PAF enzymatic assay at a high concentration. A sulfonamide fragment **10** with millimolar potency was obtained, and the binding mode was validated by its co-crystal structure with recombinant human Lp-PLA2 (rhLp-PLA2) (Figure 2). To the best of our knowledge, no sulfonamide scaffold Lp-PLA2 inhibitors were known at the time we initiated our work. With such a novel binding moiety in hand, we conducted the fragment evolution in order to obtain highly potent Lp-PLA2 inhibitors. With an invaluable aid from the crystal structure of rhLp-PLA2 in complex with fragment **10**, a virtual screening strategy was employed. Firstly, a similarity search was performed, and compounds containing fragment **10** were subsequently subjected to a docking study. The selected hits were purchased and assessed with the PAF enzymatic assay, resulting in

a micromolar inhibitor **11**. Guided by the crystal structures of rhLp-PLA2 bound with these novel compounds, several low nanomolar inhibitors were obtained through a hit-to-lead optimization. Herein, we will clearly illustrate how this efficient lead discovery, from a rather weak binder to a series of nanomolar inhibitors, is accomplished.

RESULTS AND DISCUSSION

Fragment screening and validation. Fragments characterized by small size and simple structure could provide much broader chemical diversity, afford novel binding moieties of interested targets, and possess good ligand efficiency. After screening our in-house 500-fragment library, a small sulfonamide fragment **10** (MW= 207; IC_{50} = ~1mM, Figure 2) was obtained and it afforded efficient binding to rhLp-PLA2 (LE $\approx$ 0.30[24]). The crystal structure shows that it, exhibiting with unambiguous electron density (Figure S1A), occupies the center of the ligand binding pocket and bridges residues comprising the oxyanion hole[2a] to those near the lipoprotein binding helices[25] (Figure 2), thereby exerting an influence on the full binding pocket of Lp-PLA2. The methylsulfonamide tail of fragment **10** interacts with the catalytic sub-pocket by forming multiple direct and/or water-bridged hydrogen-bonds (H-bonds) with surrounding residues. The amide nitrogen in the side-chain of Gln352 serves as a H-bond donor to one of the sulfonamide oxygen (**O1**). Meanwhile carbonyl oxygen in this side chain is linked to residues (Phe357 and Thr358) near the lipoprotein binding helices via a water molecule (W2). The second sulfonamide oxygen (**O2**) bonds the hydroxyl group of the

catalytic residue Ser273 and another crucial water molecule (W1) located in the oxyanion hole[2a]. The last H-bond is established between the main-chain carbonyl oxygen of Leu153 and the NH group linked to the sulfonamide tail. In addition, the 3,4-difluorophenyl group of fragment **10** is buried into a hydrophobic sub-pocket consisting of residues Leu107, Phe110, Gly154, Ala155, and Leu159, contributing to the efficient binding of this fragment to Lp-PLA2.

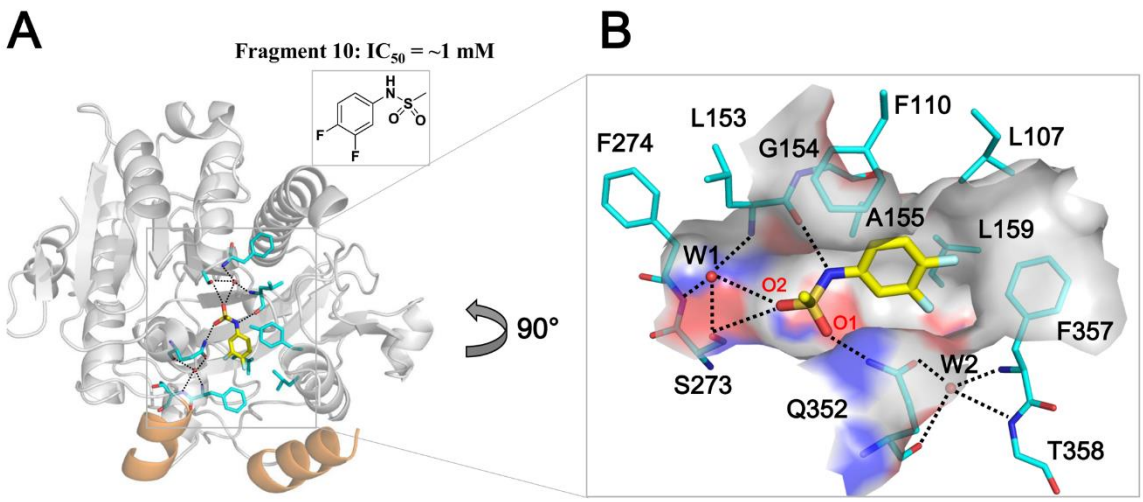

Figure 2 The crystal structure of rhLp-PLA2 in complex with fragment **10** (PDB ID: 5YE8). (A) An overall view of the complex structure. Lp-PLA2 is shown as gray cartoon. Two lipoprotein binding helices (residues 114-126 and 362-369) are colored in orange. (B) A close-up view of fragment **10** within the binding pocket which is presented by molecular surface. H-bonds are represented by black dashed lines. Fragment **10** (yellow) and the surrounding residues (cyan) are shown as sticks. Two water molecules (W1 and W2) are shown as red spheres.

Virtual screening and hit identification. Inspired by the elegant binding of

fragment **10** with the protein, we carried out fragment optimization to enhance the binding affinity to Lp-PLA2. A similarity search was first performed with the SPECS database and subsequently a molecular docking of the compounds containing the *N*-phenylsulfonamide core into the ligand binding pocket of Lp-PLA2 was conducted. The 500 highest-ranking compounds resulted from the virtual screening were visually inspected and those with distinct binding modes compared to fragment **10** were discarded. The survivors were then imported into the Schrödinger program Canvas for clustering analysis using the Leader-Follower method. Ultimately, 100 compounds with diverse structures were purchased and tested with the PAF enzymatic assay. Compound **11** representing low micromolar inhibitory activity (IC_{50} = 3431 nM, Table 1) was identified as a promising hit.

To elucidate the significant inhibitory activity improvement and guide further optimization, we determined the X-ray crystal structure of compound **11** binding with rhLp-PLA2. Compound **11** is superimposed perfectly on fragment **10** and almost all the aforementioned protein-ligand interactions are conserved (Figure 3A). Furthermore, the *N*-phenylacetamide group and the diaryl ether moiety of **11** expand along the canyon-like groove in two opposite directions. The *N*-phenylacetamide group projects into the solvent-accessible region nearby the catalytic site and forms hydrophobic interactions with Phe110. In this case, the side-chain of Gln352 is slightly changed compared to its conformation in the Lp-PLA2-**10** structure, disrupting the aforementioned water-mediated network among Gln352, Phe357 and Thr358. The naphthyl group of

compound **11** sits above the lipoprotein binding helices at the other side and it is surrounded by hydrophobic residues Leu111, Phe357, Leu369, and Leu371. It is noticed that the electron density of the terminal benzene ring of the naphthyl group is partially missing (Figure S1B), indicating that it may not perfectly fit into this sub-pocket.

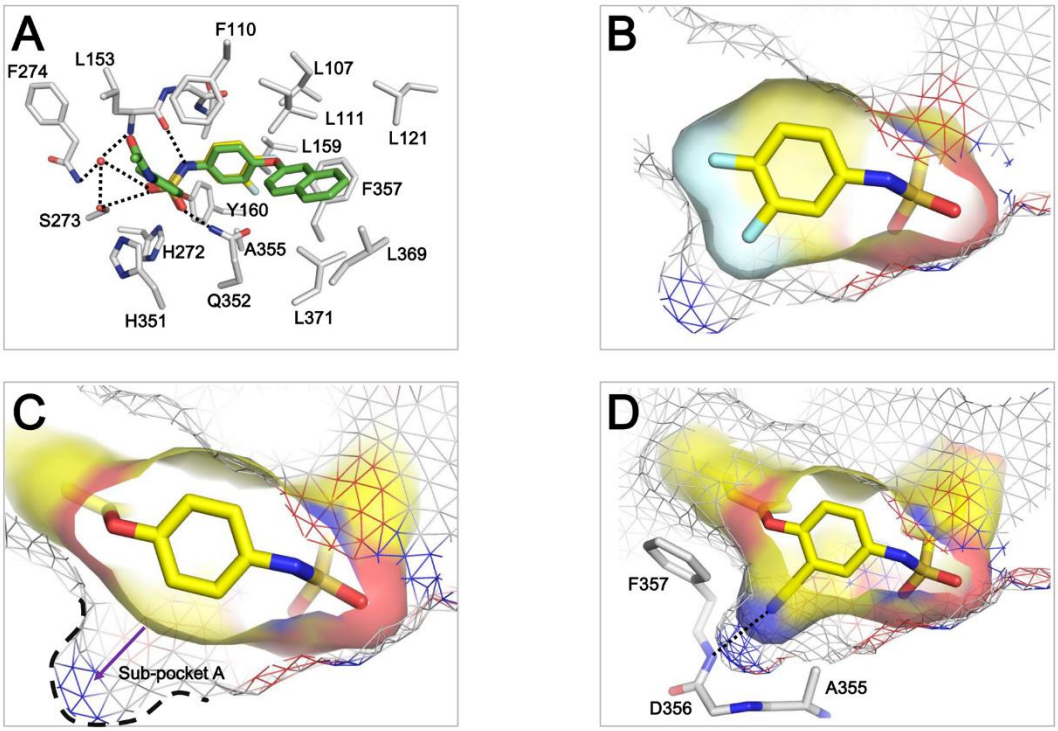

Figure 3. (A) Superimposed crystal structures of compound **11** (green sticks) and **10** (yellow sticks) in complex with rhLp-PLA2. Residues interacting with compound **11** are shown as gray sticks, and H-bonds are represented by black dashed lines. (B-D) A surface representation of **10** (B, PDB ID: 5YE8), **11** (C, PDB ID: 5YE7) and **14a** (D, PDB ID: 5YE9) from the opposite view (180 ° rotation) of (A). The ligand binding pockets are shown with gray meshes. The sub-pocket A is marked in (C) with black dashed lines and the purple arrow highlights the growing direction at the 3-position of the central benzene

ring of compound **11**.

Structure optimization and SAR. Elaboration of hit **11** was initiated by exploring the *N*-phenylsulfonamide binding core derived from fragment **10**. After a comparative investigation on complex structures of Lp-PLA2 bound with **10** and **11**, we deduced that a small sub-pocket (sub-pocket A) proximal to the middle benzene ring of **11** could be utilized and different substitutes (R_1) were thereby explored by increasing the size from the smallest fluorine to a methoxyl group (Figure 3 and Table 1). The synthesized compounds, at concentrations of 25 μM and 2.5 μM, were tested with the PAF enzymatic assay, and compounds with stronger potency compared to **11** were subjected to IC_{50} measurement. It turns out that a fluorine substitution of R_1 (compound **12**) displays two-fold potency improvement, verifying the rationale of our optimization strategy. Compounds **13a** and **15a** decorated with a bulkier chlorine and methyl group, respectively, alleviate the inhibition of the enzyme compared to **11**. While a trifluoromethyl (**16a**) or methoxyl (**17a**) substituent is unlike to be tolerated at the sub-pocket A as they almost completely lost their inhibitory activity at 25 μM. Remarkably, when a linear cyano group was attached to R_1, compound **14a** displays a 10-fold potency improvement compared to **11**. It is thus suggested that the sub-pocket A could only accommodate a narrow and short group like fluorine or cyano. In addition, compatible with the complex structure, compounds with different R_2 substitutions all lose their potencies against rhLp-PLA2 (Table S1), since there is no space to accommodate

these groups (Figure 3B-D). Accordingly, introduction of substituents to fill the narrow space between the inhibitor and the binding pocket should be very careful.

Table 1. Effects of R_1 on inhibitory activity of rhLp-PLA2.

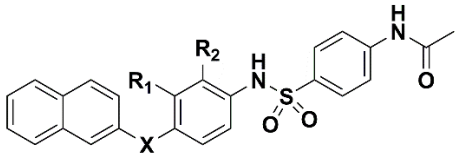

Compd	R_1	R_2	X	% inhibition rhLp-PLA2		IC_{50} (nM)
				25 μM	2.5 μM	
11	H	H	O	85	38	3431
12	F	H	O	93	59	1418
13a	Cl	H	O	82	8	
14a	CN	H	O	100	100	355
15a	CH_3	H	O	75	25	
16a	CF_3	H	O	13	0	
17a	OCH_3	H	O	0	0	
18	CN	H	S	99	30	
19	CN	H	NH	87	53	1915
20	CN	H	NCH_3	45	0	

Additionally, a linker between the *N*-phenylsulfonamide core and the terminal naphthalene ring was investigated based on compound **14a**. Replacement of the oxygen atom with a sulfur (**18**) or nitrogen (**19**) both resulted in a remarkably reduced potency. When a methyl group was attached to the nitrogen linker, compound **20** also loses its

inhibition of rhLp-PLA2. Therefore, the oxygen may be the best option for this linker.

Table 2. Effects of R_3 and R_4 on inhibitory activity of rhLp-PLA2.

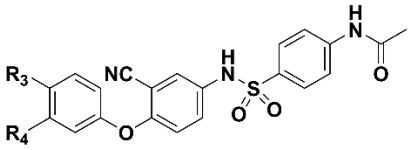

Compd	R_3	R_4	IC_{50} (nM)
14a			355
21	H	H	2477
22	F	H	1070
23	Cl	H	322
24	CN	H	613
25	Cl	F	222
26	Cl	Cl	45
27	Cl	CN	152
28	Cl	CH_3	100
29	Cl	CF_3	17
30	Cl	OCH_3	924
31	Cl	benzyl	902
31a	Cl	phenyl	1027
32	F	CF_3	45
33	CN	CF_3	23

Based on the results above, compound **14a** was selected for further optimization, and the crystal structure of **14a** in complex with rhLp-PLA2 was determined. Similar to the fluorine at the 3-position of fragment **10**, the cyano group of **14a** fits well into the

sub-pocket A, forming a H-bond with the main-chain nitrogen of Phe357 and hydrophobic interactions with Ala355 and Phe357 (Figure 3D), both of which render it more potent than compound **11**. Like compound **11**, the electron density of the terminal benzene ring of the naphthyl group in the complex structure is not completed (Figure S1C), leading us to believe that this ring is not comfortable in the binding pocket. Unexpectedly, converting the naphthyl to a phenyl group results in compound **21** with an IC_{50} of 2477 nM, ~8-fold weaker in the potency, which indicates that this terminal benzene ring is indeed dedicated to the ligand binding to Lp-PLA2 despite of the uncompleted electron density.

In order to refill this binding site, substituent exploration on terminal benzene ring of **21** was therefore conducted (Table 2). Deciphered from the complex structure of **14a** bound with rhLp-PLA2, the two ortho-positions of the ether bond in the naphthyl group are in close proximity with Gln352, Phe357 and Leu107 (Figure S2), suggesting that these positions are not suitable for substituent exploration. Learning the experience from R_2 substitution, we only investigated the para- and meta-substituents (R_3 and R_4) based on compound **21**. Empirically, the para-position of the terminal benzene ring (R_3) in **21** tends to be oxidatively metabolized into a benzoquinone. We primarily introduced a fluorine, chlorine or cyano group (**22-24**) to block the para-position. The chlorine substituent (**23**) restores the activity of **14a**, and the cyano (**24**) or fluorine (**22**) substitution also enhance the potency compared to **21**. Encouraged by these data, we evaluated the substitution in R_4 based on compound **23**. As shown in Table 2, the

meta-position of the terminal benzene ring prefers lipophilic substituents with an appropriate size. Larger groups like methoxy (**30**), phenyl (**31a**), or benzyl (**31**) ones decrease the inhibitory activity by three folds. Smaller substituents such as the fluorine (**25**), chlorine (**26**), cyano (**27**), methyl (**28**) and the trifluoromethyl (**29**) are propitious to affinity improvement. Especially the trifluoromethyl substitute **29** displays 20-fold potency improvement compared to **14a**. In addition, a fluorine (**32**) or cyano (**33**) substitution at the para-position renders the compound less potent compared to its chlorine analogue (**29**). In summary, after two rounds of optimization, two-digital nanomolar Lp-PLA2 inhibitors (**26**, **29**, **32**, and **33**) were identified.

Lastly, substitutions on the solvent-exposed benzene ring were carried out (Table 3). Inhibitor **29**, displaying the most potent inhibitory activity to rhLp-PLA2, was selected as the starting point for further optimization. Neither meta- nor ortho-position analogue shows better activity compared to **29** (Table S2), thus we focused on the exploration of the para-position substituents on the right benzene ring. Removing the 4-position substituent leads to compound **34** with a lipophilic phenyl group facing to the solvent, showing ~4-fold potency drop compared to **29**. Moreover, replacement of the *N*-acetyl amino group with a hydrophobic methyl (**35**) or nitro (**36**) group further weakens their binding affinities to rhLp-PLA2. All of these stated above indicate that the lipophilic moieties are not favorable in this solvent-exposed region. Unsubstituted (**37**), monosubstituted (**29**), and disubstituted (**38**) amino groups on R_5 are generally acceptable as they exhibit comparable activities. In addition, the linker between the *N*-acetyl amino

group and the right benzene ring of **29** was also explored. A single methylene elongation analogue **39** displays slight improvement in the inhibition of rhLp-PLA2, and further elongation of this linker with an ethylidene or *n*-propylidene does not enhance the potency compared to **39** (Table S2). A heterocyclic substituent such as morphine (**42**) or piperazine (**43**) results in unfavorable binding to the enzyme. Replacing the *N*-acetyl group in **29** with a morphine-4-carbamoyl group (**40**) hardly has effect on the potency. Based on these results, we surmise that the catenulate linker for extending the hydrophilic substituents of R_5 is preferable. To our surprise, the carboxyl analogue **41** outstands from this series and performs the best inhibitory activity (IC_{50}=5 nM) against rhLp-PLA2.

Table 3. Effects of R_5 on inhibitory activity of rhLp-PLA2.

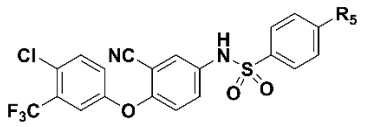

Compd	R_5	rhLp-PLA2 IC_{50}(nM)
29		17
34	H	65
35	CH_3	232
36	NO_2	236
37	NH_2	14
38		12
39		9
40	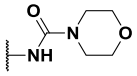	13
41	COOH	5
42	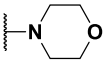	42
43	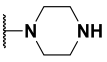	57
Darapladib	/	0.6

The crystal structure of compound **41** in complex with rhLp-PLA2 was determined to elucidate the structure basis underlying its high potency. This time the electron density of the bounded compound is clear and completed as well (Figure S1D). In addition, the

ortho-positions of the ether bond in the terminal benzene ring are close to Lp-PLA2 binding pocket and indeed have no space to be decorated. Analogously, the sulfonamide oxygen forms H-bonding interactions with Phe274, Ser273 and Leu153 (Figure 4). The additional H-bond is established between the CN group of **41** and the main-chain of Phe357. Noteworthy, in the complex structure of Lp-PLA2-**41**, the side-chain of Gln352 rotated 90 ° from that in the complex structure with fragment **10**, resulting in another ordered conformation mediated by two H-bonds with Lys370 and a water molecule (Figure 4). In contrast, in the fragment **10** bound complex structure, the side-chain of Gln352 is oriented by the sulfonamide oxygen (**O1**) and a water molecule (W2) connecting the main-chains of Gln352, Phe357 and Thr358 (Figure 2B). Upon binding with compounds **11** and **14a**, this originally ordered conformation of Gln352 is disrupted, while the binding of compound **41** further induces Gln352 to form a new ordered conformation. Hydrophobic interactions, mainly formed between the 4-chloro-3-(trifluoromethyl) phenyl moiety and residues Phe357, Leu371, Leu111, and Leu121, also contribute to the binding affinity. Accordingly, multiple H-bonds as well as hydrophobic interactions of compound **41** with the surrounding residues account for its high inhibition of rhLp-PLA2.

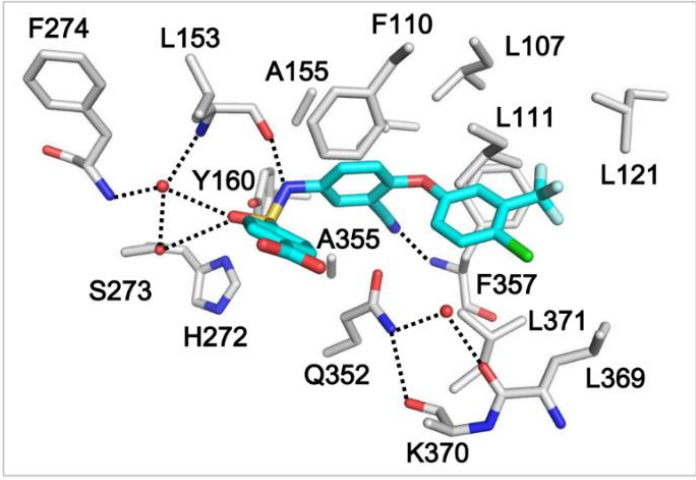

Figure 4. The detailed interactions of compound **41** with rhLp-PLA2 revealed by the crystal structure (PDB ID: 5YEA). H-bonds between residues and **41** are presented by black dashed lines.

Selectivity, plasma enzyme inhibition, rat hepatocytes stability and permeability assessment. PLA2VIIB is an intracellular phospholipase and shares 62% sequence similarity with Lp-PLA2.[26] The inhibitory activity of PLA2VIIB was measured to assess the selectivity of Lp-PLA2 inhibitors.[22-23] Overall, our Lp-PLA2 inhibitors show good selectivity (more than 1000 folds) over PLA2VIIB (Table 4).

Subsequently, the inhibitory activity of the compounds against human and rat plasma Lp-PLA2 was tested in order to select compounds for inhibition assessment *in vivo*. Compounds **37**, **39**, **40**, and **43** exhibit more than 50% inhibition of Lp-PLA2 in human plasma at a concentration of 50 nM (Table 4). For the rat plasma Lp-PLA2, compounds **39, 37**, **41,** and **43** displays relatively good inhibition (>30% at 50 nM).

The Caco-2 cell permeability measurement implies that selected compounds possess good permeability *in vitro* (Table 4). However, the high efflux ratio of **39** (11.7) was found. In the rat hepatocytes stability assay[27], compound **39** with a single methylene spacer displays a relatively poor stability, though it is the most potent inhibitor of the plasma Lp-PLA2. Given the high stability of **29**, the high CLint values of **38** (157.33 mL/min/kg) and **39** (186.36 mL/min/kg) might be due to the *N*-dealkylation of these two compounds. Other inhibitors (**29**, **32**, **33**, **37**, **40**, and **41**) show good stability in rat hepatocytes.

Table 4. Selectivity, plasma enzyme inhibition, stability and permeability of selected compounds.

Compd	PLA2VIIB	Human plasma (% @ nM)		Rat plasma (% @ nM)		Rat Hepatocytes Stability	Caco-2 Permeability	
	IC_{50}(μM)	250	50	250	50	CL_{int} (mL/min/kg)	A To B (10^{-6} cm/s)	Efflux Ratio
29	>25	56	23	64	32	NC[a]	9.5	0.8
32	>25	43	14	55	23	5.1	14.9	1.0
33	>25	37	8	42	11	0.9	9.0	1.9
37	>25	85	62	67	33	14.9	5.7	0.4
38	>25	63	29	45	15	157.3	4.4	2.4
39	>25	85	64	80	51	186.3	1.1	11.7
40	>25	82	55	64	27	NC[a]	3.8	1.9
41	>25	65	28	67	31	5.1	0.5	1.9
42	>25	41	14	48	17			
43	>25	80	57	68	31			
Darapladib	2	100	93	97	98			

[a]NC= cannot be calculated: CLint value was too low to be calculated.

***In vivo* assessment of inhibitors.** Compounds **37** and **41**, with acceptable inhibitory activities against the plasma enzyme and good stability as well as permeability *in vitro*,

were selected to assess their pharmacokinetics and potencies in the male SD rats. To determine the bioavailability, **37** and **41** were dosed at 1 mg/kg and 3 mg/kg, respectively, for intravenous and oral administration (Table 5). Though **41** displays a poor oral bioavailability (F=8.8%), compound **37** obtains excellent clearance (4.9 mL/min/kg), favorable AUC value (3.4 μg·h/mL), and good oral bioavailability (F = 35.5%).

Table 5 Pharmacokinetic profiles of 37 and 41 in male SD Rats[a]

Compd	Route	Dose (mg/kg)	CL (ml/min/kg)	V_{ss} (L/kg)	T_{max} (h)	C_{max} (μg /ml)	$T_{1/2}$ (h)	AUC_{0-24h} (μg·h/ml)	F (%)
37	IV	1	4.9	2.9			7.1	3.2	
	PO	3			4	0.27	7.7	3.4	35.5
41	IV	1	3.1	0.3			2.7	6.2	
	PO	3			0.25	0.49	2.7	1.6	8.8

[a]n = 5 animals/ group, data are the mean values.

Compounds **37**, **41** and darapladib were orally administrated at doses of 3 mg/kg and 25 mg/kg to evaluate the inhibitory potency *in vivo*. The inhibitory activity and plasma concentration of **37** and **41** are dose-dependent (Figures S3-S4) and the results of 25 mg/kg dose are presented in Figure 5A. Although **41** displays better inhibitory activity compared to darapladib in the first four hours, its potency dramatically decreases during the next four hours. However, compound **37** maintains the inhibitory activity for 24 hours after oral administration, which is superior to that of darapladib. The concentration-time curves of **37** and **41** *in vivo* (Figure 5B) may account for their distinct activities, as the

concentration of **41** reduces almost 10-fold from four hours to eight hours after being orally dosed, while compound **37** owns high concentrations in plasma for twenty-four hours. And the quick inhibition of Lp-PLA2 by **41** may benefit from its fast absorption (T_{max}=0.25 h). In addition, compound **37** displays better inhibition of the enzyme compared to darapladib at 3 mg/kg dose concentration (Figure S4). Overall, **37** is identified as a potential candidate for further development.

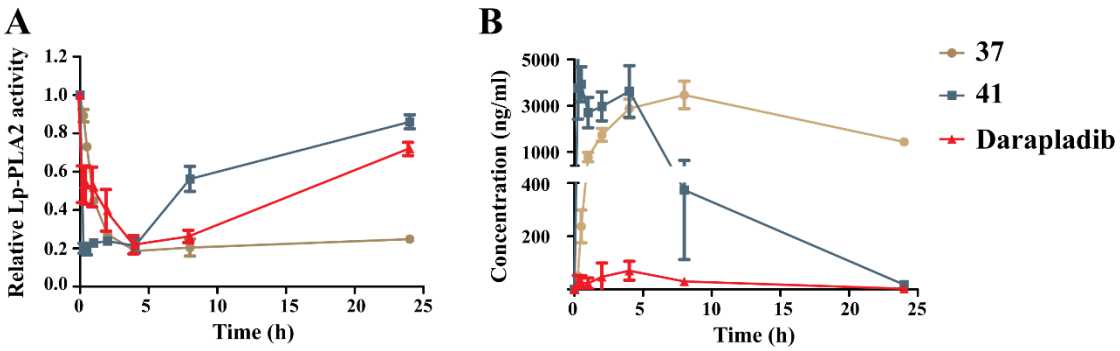

Figure 5. (A) The relative activity of Lp-PLA2 in the plasma of SD rats after an oral dose of **37**, **41** and darapladib at 25 mg/kg (n=5). For clearly representing the plasma concentration of darapladib, two different scales are displayed in (B) (bottom: 200 intervals; top: 2000 intervals), concentration-time curves of **37**, **41** and darapladib at 25 mg/kg (n=5), and all data are represented. Error bars represent the SD.

Chemistry. Synthetic route for the target compounds (**11-33**) is shown in Scheme 1. The nucleophilic substitution was firstly employed to get intermediates **44a-44o** and **46a-46n**, followed by reduction with iron powder to yield the corresponding aniline derivatives **45a-45o** and **47a-47n**, respectively. Then these intermediates reacted with

4-acetamidobenzenesulfonyl chloride in pyridine to give the desirable compounds.

Scheme 1. Synthesis of compounds **11-33**[a].

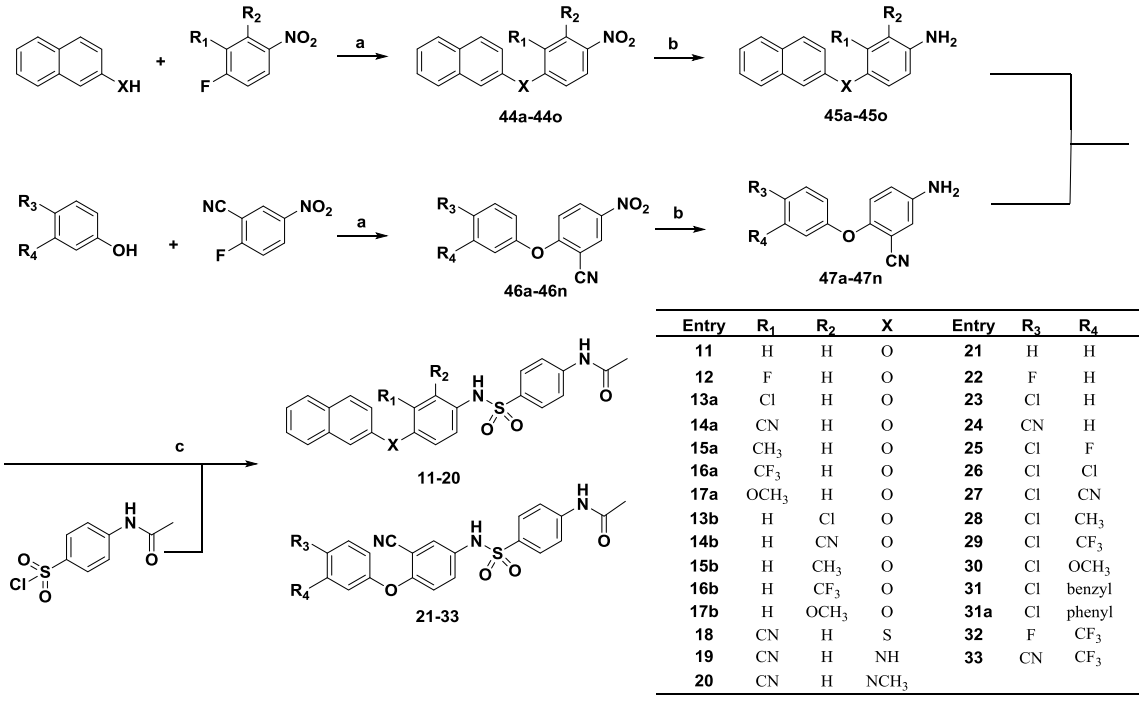

Entry	R_1	R_2	X	Entry	R_3	R_4
11	H	H	O	**21**	H	H
12	F	H	O	**22**	F	H
13a	Cl	H	O	**23**	Cl	H
14a	CN	H	O	**24**	CN	H
15a	CH_3	H	O	**25**	Cl	F
16a	CF_3	H	O	**26**	Cl	Cl
17a	OCH_3	H	O	**27**	Cl	CN
13b	H	Cl	O	**28**	Cl	CH_3
14b	H	CN	O	**29**	Cl	CF_3
15b	H	CH_3	O	**30**	Cl	OCH_3
16b	H	CF_3	O	**31**	Cl	benzyl
17b	H	OCH_3	O	**31a**	Cl	phenyl
18	CN	H	S	**32**	F	CF_3
19	CN	H	NH	**33**	CN	CF_3
20	CN	H	NCH_3			

[a]Reagents and Conditions : (a) K_2CO_3, DMF, 80 ℃, 2h; (b) EtOH/H_2O/AcOH= 10:10:1, iron powder, 75 ℃, 2h; (c) pyridine, rt, overnight.

The target compounds **34-43** and **49** were prepared from **47i** under similar conditions as that for preparation of **11-33** (Scheme 2). Among these, compounds **34-41** and **49** were obtained through an electrophilic aromatic substitution of chlorosulfonic acid (detailed procedures shown in Supporting Information). In addition, **36** was reduced to give **37**, and the fluorine in **49** was substituted by two heterocyclic groups to generate **42** and **43,** respectively.

Scheme 2. Synthesis of compounds **34-43** and **49**[a].

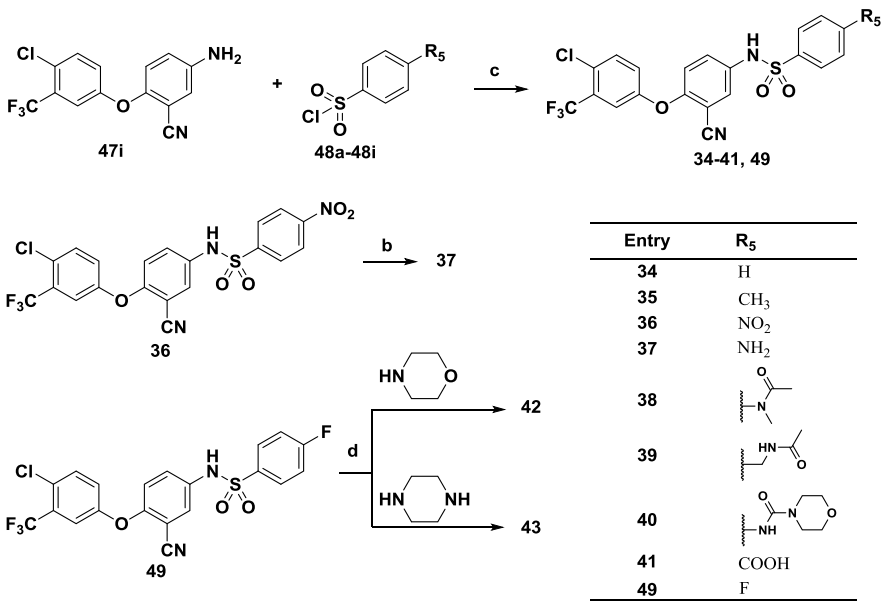

Entry	R_5
34	H
35	CH_3
36	NO_2
37	NH_2
38	
39	
40	
41	COOH
49	F

[a] Reagents and Conditions : (b) EtOH/H_2O/AcOH= 10:10:1, iron powder, 75 ℃, 2h; (c) pyridine, rt, overnight. (d) DMSO, 120 ℃, 10h.

CONCLUSIONS

Here we report the efficient discovery of novel and potent Lp-PLA2 inhibitors containing a sulfonamide scaffold with the structure-guided strategy. A ~200,000-fold affinity improvement was achieved from the initial sulfonamide fragment to the most potent compound **41**. Structure-based virtual screening (gaining ~300-fold potency improvement) together with the subsequent structure-based ligand optimization (contributing ~700-fold potency improvement) significantly accelerated the hit-to-lead optimization. Most of the resulting inhibitors display good Caco-2 cell permeability and excellent rat hepatocytes stability *in vitro*. Gratifyingly, compound **37** represents good enzyme-inhibition activity and oral bioavailability in SD rats, and further optimization of this compound is now under way.

EXPERIMENTAL SECTION

PAF enzymatic assay. The inhibitory activity against the human recombinant Lp-PLA2, PLA2-VIIB or plasma Lp-PLA2 was performed according to the protocol of Chen et al[20]. The substrate 2-thio-PAF (Cayman Chemical) and 5,5′-dithiobis(2-nitrobenzoic acid), (DNTB, Sigma-Aldrich) were used to produce the absorbance at 412 nm after enzymatic reaction. The purification of recombinant Lp-PLA2 and PLA2-VIIB was presented in the Supporting Information. The recombinant and plasma Lp-PLA2 were added to the enzymatic system directly. 5 μL compound, 10 μL 2 mM DNTB and 10 μL protein/ plasma were incubated for 30 min at room temperature. Finally, 175 μL substrate solution (50 mM Tris pH 7.2, 1 mM EGTA, 50 μM 2-S-PAF) was added to the enzymatic system. Enzymatic kinetics were measured every minute of 10-min reaction time and Vmax was obtained to measure the inhibition. The IC_{50} curves were generated using GraphPad Prism[28] and each IC_{50} value was replicated at least three times.

This study has been approved and supervised by Institutional Animal Care and Use Committee (IACUC), Shanghai Institute of Materia Medica, Chinese Academy of Sciences (IACUC approval no.:2017-02-YY-05), and the Ethics Committee of Shanghai Blood Center.

Crystal structure determination. The purified protein was concentrated to 4 mg/ml for crystallization. Crystallization of rhLp-PLA2 was carried out by mixing a solution of the protein with an equal volume of the precipitant solution (0.1 M MOPS pH 6.6, 0.4 M

Li_2SO_4, 27% (w/v) $(NH4)_2SO_4$, 1 M Na-Ac, 1.4% (v/v) 1,4-butanediol). Crystals were obtained by the vapour-diffusion method in hanging drops at 20°C. The protein-inhibitor complex crystals were prepared by soaking crystals of apo rhLp-PLA2 into the reservoir solution containing 10 mM inhibitors or 50 mM fragments overnight. Subsequently, crystals were directly flash frozen in liquid nitrogen.

Data were collected at 100 K at the Shanghai Synchrotron Radiation Facility (SSRF)[29], and were processed with the HKL software packages[30]. The structure was solved by molecular replacement, using the program PHASER[31] with the search model of PDB ID: 5I8P[2b]. The structure was refined with the simulated-annealing protocol implemented in the program PHENIX[32]. With the aid of the program Coot[33], compounds and water molecules were fitted into the initial *Fo-Fc* map. The complete statistics, as well as the quality of four solved structures, are shown in Table S3.

Metabolic stability in rat hepatocytes. The procedures of rat hepatocytes isolation were performed in accordance with Guide for the Care and Use of Laboratory Animals at Shanghai Institute of Materia Medica, Chinese Academy of Sciences. The details for preparation of rat hepatocytes followed the classic protocol[34]. Compounds were dissolved in DMSO to a final concentration of 1.0 μM (DMSO% was less than 0.1%, v/v) and incubated with the rat hepatocytes (1.0×10^6 cells/mL) in Williams' E medium at 37°C. Aliquots were removed at 0, 0.25, 0.5, 1, 1.5, and 2 h, and the reactions were quenched with equal volume of ice-cold acetonitrile. Samples were injected to HPLC-MS/MS for analysis and each experiment was performed in duplicate.

Half-live of the compound in hepatocytes was calculated using the following equation:

$$T_{1/2} = 0.693/k$$

(-k) was the slope of the linear regression from log [substrate] versus time plot.

Intrinsic clearance was calculated using the following equation:

$$CL_{int} = 0.693 \times \text{Scaling factor} / T_{1/2} = 2.990 / T_{1/2}\ (\text{L/min·kg})$$

Scaling factors employed in this calculation:

Scaling factor = (Rat liver weight/rat body weight) × (hepatocellularity/liver weight) / (hepatocellular density in reaction system)

Rat liver weight/rat body weight = 40 g/kg; hepatocellularity/liver weight = 117×10^6 cells/g; hepatocellular density in reaction system= 1.0×10^6 cells/mL.

Caco-2 Permeability Assay. The Caco-2 monolayer assays were performed by using standard procedure as previously reported for pyrimidone derivatives[20]. Briefly, drug transport from the apical side to the basolateral side (A–B) and from the basolateral side to the apical side (B–A) was measured simultaneously under the same condition. Propranolol and nadolol were used as the hypertonic and hypotonic control, respectively. Digoxin was used as the positive control for Pgp-mediated drug efflux. After washing the monolayer with HBSS (Hanks' Balanced Salt solution, Sigma-Aldrich) three times, the compounds were diluted and added to the appropriate well (pH 6.8 for the apical side and pH 7.4 for the basolateral side). The plate was incubated at 37 ℃ for 95 min. Samples were collected from the donor side at 5 and 95 min and from the receiver side at 35 and

95 min post-incubation. The concentration of samples was measured by LC-MS/MS. The P_{app} was calculated from the following equation:

$$P_{app} = \frac{V_A}{S_A \times T} \times \frac{[drug]_{acceptor}}{[drug]_{initial\ donor}}$$

Where V_A is the volume of the acceptor well, S_A is the surface area of the membrane, T is the total transport time, $[drug]_{acceptor}$ is the drug level at the acceptor side, and $[drug]_{initial\ donor}$ is the drug level at the donor side at T = 0.

Animals. Male Sprague-Dawley (SD) rats (180- 220g for compound **37** and darapladib, 200- 250g for **41**, supplied by Shanghai experimental animal center, CAS) with five animals in each group were used for the *in vivo* studies. Animal experiments were approved and supervised by Institutional Animal Care and Use Committee (IACUC), Shanghai Institute of Materia Medica, Chinese Academy of Sciences (IACUC approval no.:2017-02-YY-05).

***In vivo* study of selected compounds.** Compounds dissolved in DMSO/0.25% carboxymethylcellulose sodium (5/95, v/v) were subjected to oral administration at doses of 3 mg/kg and 25 mg/kg. For the IV route, a group of five male SD rats were injected with a single dose of 1 mg/kg with a dose volume of 5 mL/kg using PEG300/EtOH/saline (40/10/50, v/v/v) as the vehicle. For both routes, serial specimens were collected predose as well as 0.25, 0.5, 1, 2, 4, 8, and 24 h after administration. For pharmacokinetic analysis, samples (except for the predose specimens) were precipitated with MeOH/acetonitrile (1:1, v/v) and quantified by HPLC-MS. Pharmacokinetic parameters were calculated from the mean serum concentration by non-compartmental analyses (MassLynx V4.1,

Waters).

For the *in vivo* activity analysis, blood samples, drawn predose as well as 0.25, 0.5, 1, 2, 4, 8, and 24 h after administration, were applied to measure the Lp-PLA2 activity in plasma. The Lp-PLA2 activity in the plasma of SD rats was measured by using the same protocol as that used for measurement of Lp-PLA2 inhibitory activity *in vitro*.

Synthetic Chemistry. All reagents were purchased from commercial suppliers and used without further drying or purification unless otherwise stated. Yields were not optimized. ^{1}H NMR and ^{13}C NMR spectra were recorded on a Bruker AC400 or a Bruker AC500 NMR spectrometer using tetramethylsilane as an internal reference. Low-resolution mass spectra were determined on an Agilent liquid-chromatography mass spectrometer system that consisted of an Agilent 1260 infinity LC coupled to Agilent 6120 Quadrupole mass spectrometer (ESI). High-resolution mass spectra were conducted on a triple TOF 5600^{+} MS/MS system (AB Sciex, Concord, Ontario, Canada) in the negative or positive ESI mode. The purity of test compounds were determined by HPLC (Agilent ChemStation, Agilent Eclipse XDB-C18, 5 μM, 4.6×150 mm, 30 °C, UV 240 nM, flow rate = 1.0 mL/min) with aqueous CH_3CN (30%−90%, 0.1% FA only for compound **43**) for 12 min. All the assayed compounds possess ≥95% purity. Column chromatography was performed on silica gel (200−300 mesh) or with pre-packed silica cartridges (4-40g) from Bonna-Agela Technologies Inc. (Tianjin, China) and eluted with a CombiFlash@ Rf 200 from Teledyne Isco, and preparative TLC was performed on HSGF 254 (0.4−0.5 mm thickness; Yantai Jiangyou Company, Yantai, Shangdong, China).

General Procedure 1. Step **a**: Dissolving the *p*-fluoronitrobenzene or its derivative (0.1 mM) in DMF, then K_2CO_3 (0.13 mM) and corresponding nucleophilic reagent (0.1 mM) were added, and the mixture was heated at 80 ℃ for 2h. The reaction was quenched with water and the product was extracted with EtOAc (×3). The organic layer was washed with saturated NaCl solution (×3) and dried with anhydrous magnesium sulfate. The extracting solvent was evaporated in vacuo, and the residue was directly for the next step without purification.

Step **b**: The residue obtained (0.1 mM) from above step was dissolved in EtOH:H_2O:AcOH (v:v:v = 10:10:1). After being added with reduced iron powder (0.5 mM), the solution was heated to 75 ℃ for 2h. Then it was diluted with EtOAc and the water layer was extracted with EtOAc for another 2 times. The organic layer was combined, washed with brine, dried with anhydrous $MgSO_4$, filtered, and evaporated in vacuo. The residue was purified by column chromatography (PE/EA= 5:1).

General Procedure 2: Selected aniline derivative (0.1 mM) was previously dissolved in pyridine, and the corresponding sulfonyl chloride (0.11 mM) was added slowly. If the sulfonyl chloride was oil, beforehand dissolving it in THF was necessary. The mixture was stirred overnight at room temperature, concentrated to small volume in vacuo, and neutralized with 2M HCl. Then it was extracted by EtOAc for three times. The combined organic layers were washed by a saturated aqueous NaCl solution (×3), dried over $MgSO_4$, filtered, and concentrated under reduced pressure. Purification by column chromatography on silica gel (DCM/MeOH=50:1) afforded the desirable compound.

The preparation of major intermediates was according to general procedure 1, detailed information was showed in the Supporting Information. Only target compounds were displayed here.

*N-(3,4-difluorophenyl)methanesulfonamide (**10**).* Commercially purchased. ^{1}H NMR (400 MHz, DMSO-d_6) δ 9.93 (s, 1H), 7.38 (dt, J = 10.6, 9.1 Hz, 1H), 7.20 (ddd, J = 12.3, 7.2, 2.6 Hz, 1H), 7.05 – 6.98 (m, 1H), 3.01 (s, 3H).^{13}C NMR (126 MHz, DMSO-d_6) δ 149.40 (dd, J = 245.3, 13.4 Hz), 146.24 (dd, J = 242.0, 12.5 Hz), 135.38 (dd, J = 8.5, 2.7 Hz), 117.98 (d, J = 18.0 Hz), 116.45 (dd, J = 6.1, 3.3 Hz), 109.19 (d, J = 20.5 Hz), 39.30 . HRMS (ESI): *m/z* [M-H]$^-$ calculated for $C_7H_6F_2NO_2S^-$, 206.0093; found, 206.0086.

*N-(4-(N-(4-(naphthalen-2-yloxy)phenyl)sulfamoyl)phenyl)acetamide (**11**).* Starting with 4-acetamidobenzenesulfonyl chloride and **45a**, **11** was obtained as a white solid by using general procedure 2 (yield 76%). ^{1}H NMR (400 MHz, DMSO-d_6) δ 10.32 (s, 1H), 10.10 (s, 1H), 7.92 (d, J = 8.8 Hz, 1H), 7.88 (d, J = 8.0 Hz, 1H), 7.79 – 7.66 (m, 5H), 7.49 – 7.38 (m, 2H), 7.26 – 7.20 (m, 2H), 7.14 – 7.07 (m, 2H), 7.02 – 6.95 (m, 2H), 2.07 (s, 3H).^{13}C NMR (101 MHz, DMSO-d_6) δ 169.02 , 154.85 , 152.92 , 143.12 , 133.87 , 133.55 , 132.93 , 130.06 , 129.65 , 127.97 (2C), 127.61 , 127.00 , 126.64 , 124.74 , 122.75 (2C), 119.85 (2C), 119.40 , 118.51 (2C), 112.97 , 24.13 . HRMS (ESI): *m/z* [M--H]$^-$ calculated for $C_{24}H_{19}N_2O_4S^-$, 431.1071; found, 431.1074.

*N-(4-(N-(3-fluoro-4-(naphthalen-2-yloxy)phenyl)sulfamoyl)phenyl)acetamide (**12**).* According to general procedure 2, the white solid **12** was got from **45b** and 4-acetamidobenzenesulfonyl chloride (yield 72%).^{1}H NMR (400 MHz, DMSO-d_6) δ

10.51 (s, 1H), 10.38 (s, 1H), 7.91 – 7.80 (m, 6H), 7.72 (d, *J* = 8.1 Hz, 1H), 7.47 – 7.34 (m, 2H), 7.29 – 7.14 (m, 4H), 7.03 (d, *J* = 10.0 Hz, 1H), 2.10 (s, 3H). ^{13}C NMR (126 MHz, DMSO-d_6) δ 169.12 , 155.15 , 153.64 (d, *J* = 247.1 Hz), 143.50 , 138.68 (d, *J* = 11.7 Hz), 135.62 (d, *J* = 9.2 Hz), 133.80 , 132.70 , 130.10 , 129.62 , 128.15 (2C), 127.61 , 127.00 , 126.73 , 124.71 , 123.28 , 118.75 (2C), 118.19 , 116.93 , 110.92 , 109.15 (d, *J* = 21.8 Hz), 24.17 .HRMS (ESI): *m/z* [M-H]$^-$ calculated for $C_{24}H_{18}FN_2O_4S^-$, 449.0977; found, 449.0979.

N-(4-(N-(3-chloro-4-(naphthalen-2-yloxy)phenyl)sulfamoyl)phenyl)acetamide ***(13a)***. Starting with 4-acetamidobenzenesulfonyl chloride and **45c**, **13a** was obtained as a white solid by using general procedure 2 (yield 66%). ^{1}H NMR (400 MHz, DMSO-d_6) δ 10.36 (s, 1H), 10.33 (br s, 1H), 7.92 (d, *J* = 9.0 Hz, 1H), 7.87 (d, *J* = 7.9 Hz, 1H), 7.81 – 7.70 (m, 5H), 7.49 – 7.37 (m, 2H), 7.32 – 7.27 (m, 1H), 7.23 (dd, *J* = 8.9, 2.5 Hz, 1H), 7.15 – 7.06 (m, 3H), 2.08 (s, 3H).^{13}C NMR (126 MHz, DMSO-d_6) δ 169.08 , 154.67 , 147.47 , 143.38 , 135.35 , 133.77 , 132.59 , 130.18 , 129.63 , 128.04（2C）, 127.61 , 127.00 , 126.74 , 125.28 , 124.77 , 122.58 , 122.03 , 120.66 , 118.65（2C）, 118.46 , 111.44 , 24.14 .HRMS (ESI): *m/z* [M-H]$^-$ calculated for $C_{24}H_{18}ClN_2O_4S^-$, 465.0681; found, 465.0685.

N-(4-(N-(3-cyano-4-(naphthalen-2-yloxy)phenyl)sulfamoyl)phenyl)acetamide ***(14a)***. According to general procedure 2, the white solid **14a** was got from **45d** and 4-acetamidobenzenesulfonyl chloride (yield 75%). ^{1}H NMR (400 MHz, DMSO-d_6) δ 10.46 (br s, 1H), 10.36 (s, 1H), 7.98 (d, *J* = 8.9 Hz, 1H), 7.92 (d, *J* = 7.7 Hz, 1H), 7.83 (d,

J = 7.8 Hz, 1H), 7.80 – 7.70 (m, 4H), 7.55 – 7.43 (m, 4H), 7.38 – 7.28 (m, 2H), 7.01 (d, *J* = 9.1 Hz, 1H), 2.08 (s, 3H).^{13}C NMR (101 MHz, DMSO-d_6) δ 169.11 , 154.90 , 153.17 , 143.45 , 133.89 , 133.78 , 132.43 , 130.52 , 130.35 , 128.07 (2C), 127.73 , 127.56 , 127.31 , 126.89 , 125.46 , 124.96 , 119.77 , 119.42 , 118.70 (2C), 115.39 , 114.58 , 103.75 , 24.16 . HRMS (ESI): *m/z* [M-H]$^-$ calculated for $C_{25}H_{18}N_3O_4S^-$, 456.1024; found, 456.1033.

N-(4-(N-(3-methyl-4-(naphthalen-2-yloxy)phenyl)sulfamoyl)phenyl)acetamide ***(15a)***. Starting with 4-acetamidobenzenesulfonyl chloride and **45e**, **15a** was obtained as a white solid by using general procedure 2 (yield 61%). ^{1}H NMR (400 MHz, DMSO-d_6) δ 10.32 (s, 1H), 10.09 (s, 1H), 7.90 (d, *J* = 9.0 Hz, 1H), 7.86 (d, *J* = 8.0 Hz, 1H), 7.78 – 7.67 (m, 5H), 7.47 – 7.35 (m, 2H), 7.20 (dd, *J* = 8.9, 2.5 Hz, 1H), 7.07 (d, *J* = 2.4 Hz, 1H), 6.99 (d, *J* = 2.4 Hz, 1H), 6.95 (dd, *J* = 8.7, 2.5 Hz, 1H), 6.88 (d, *J* = 8.7 Hz, 1H), 2.07 (s, 6H).^{13}C NMR (101 MHz, DMSO-d6) δ 169.02 , 155.44 , 150.06 , 143.11 , 134.17 , 133.88 , 133.00 , 130.27 , 130.04 , 129.29 , 127.99 (2C), 127.59 , 126.85 , 126.64 , 124.42 , 123.72 , 120.89 , 119.84 , 118.56 , 118.50 (2C), 110.70 , 24.13 , 15.94 .HRMS (ESI): *m/z* [M-H]$^-$ calculated for $C_{25}H_{21}N_2O_4S^-$, 445.1228; found, 445.1236.

N-(4-(N-(4-(naphthalen-2-yloxy)-3-(trifluoromethyl)phenyl)sulfamoyl)phenyl)acetamide ***(16a)***. According to general procedure 2, the white solid **16a** was got from **45f** and 4-acetamidobenzenesulfonyl chloride (yield 63%). ^{1}H NMR (400 MHz, DMSO-d_6) δ 10.46 (s, 1H), 10.35 (s, 1H), 7.96 (d, *J* = 9.0 Hz, 1H), 7.91 (d, *J* = 7.9 Hz, 1H), 7.82 (d, *J* = 7.9 Hz, 1H), 7.79 – 7.67 (m, 4H), 7.53 – 7.42 (m, 3H), 7.37 – 7.31 (m, 2H), 7.24 (dd, *J*

= 8.9, 2.5 Hz, 1H), 7.07 (d, *J* = 8.9 Hz, 1H), 2.07 (s, 3H).^{13}C NMR (126 MHz, DMSO-d_6) δ 169.07 , 154.11 , 150.34 , 143.40 , 133.78 , 133.70 , 132.43 , 130.33 , 130.00 , 128.00 (2C), 127.65 , 127.17, 126.80 , 126.22, 125.16, 122.91 (q, *J* = 272.7 Hz), 121.58, 120.53(q, *J* = 30.9 Hz), 119.15 , 118.74 (q, *J* = 5.2 Hz), 118.62 (2C), 113.71 , 24.12 .HRMS (ESI): *m/z* [M-H]$^-$ calculated for $C_{25}H_{18}F_3N_2O_4S^-$, 499.0945; found, 499.0953.

N-(4-(N-(3-methoxy-4-(naphthalen-2-yloxy)phenyl)sulfamoyl)phenyl)acetamide ***(17a)***. Starting with 4-acetamidobenzenesulfonyl chloride and **45g**, **17a** was obtained as a white solid by using general procedure 2 (yield 66%).^{1}H NMR (400 MHz, DMSO-d_6) δ 10.34 (s, 1H), 10.18 (s, 1H), 7.90 – 7.82 (m, 2H), 7.80 – 7.72 (m, 4H), 7.69 (d, *J* = 8.1 Hz, 1H), 7.46 – 7.33 (m, 2H), 7.17 (dd, *J* = 8.9, 2.5 Hz, 1H), 7.00 (d, *J* = 8.5 Hz, 1H), 6.95 – 6.89 (m, 2H), 6.69 (dd, *J* = 8.5, 2.4 Hz, 1H), 3.64 (s, 3H), 2.08 (s, 3H).^{13}C NMR (101 MHz, DMSO-d_6) δ 169.04 , 155.95 , 151.54 , 143.22 , 139.67 , 135.59 , 133.82 , 132.83 , 129.70 , 129.13 , 128.13 (2C), 127.54 , 126.79 , 126.55 , 124.20 , 122.49 , 118.52 (2C), 118.09 , 112.76 , 109.66 , 106.06 , 55.61 , 24.14 .HRMS (ESI): *m/z* [M-H]$^-$ calculated for $C_{25}H_{21}N_2O_5S^-$, 461.1177; found, 461.1180.

N-(4-(N-(3-cyano-4-(naphthalen-2-ylthio)phenyl)sulfamoyl)phenyl)acetamide ***(18)***. According to general procedure 2, the white solid **18** was got from **45h** and 4-acetamidobenzenesulfonyl chloride (yield 68%). ^{1}H NMR (400 MHz, DMSO-d_6) δ 10.80 (s, 1H), 10.36 (s, 1H), 7.93 – 7.88 (m, 2H), 7.87 – 7.81 (m, 2H), 7.76 (s, 4H), 7.56 – 7.49 (m, 3H), 7.38 – 7.34 (m, 2H), 7.32 (dd, *J* = 8.6, 1.8 Hz, 1H), 2.08 (s, 3H).^{13}C

NMR (101 MHz, DMSO-d_6) δ 169.08 , 143.58 , 138.27 , 134.10 , 133.32 , 132.58 , 132.24 , 132.07 , 130.47 , 129.72 , 129.47 , 128.08 (2C), 127.85 , 127.68 , 127.46 , 127.00 , 126.83 , 124.57 , 123.75 , 118.71 (2C), 116.43 , 114.87 , 24.15 .HRMS (ESI): *m/z* $[M-H]^-$ calculated for $C_{25}H_{18}N_3O_3S_2^-$, 472.0795; found, 472.0806.

N-(4-(N-(3-cyano-4-(naphthalen-2-ylamino)phenyl)sulfamoyl)phenyl)acetamide ***(19)***. Starting with 4-acetamidobenzenesulfonyl chloride and **45i**, **19** was obtained as a yellow solid by using general procedure 2 (yield 71%).^{1}H NMR (400 MHz, DMSO-d_6) δ 10.33 (s, 1H), 10.18 (s, 1H), 8.59 (s, 1H), 7.82 – 7.67 (m, 7H), 7.42 – 7.23 (m, 7H), 2.07 (s, 3H).^{13}C NMR (126 MHz, DMSO-d_6) δ 169.08 , 143.29 , 143.20 , 140.30 , 134.00 , 132.62 , 131.23 , 128.98 , 128.94 , 128.01 (2C), 127.87 , 127.49 , 126.51 , 126.36 , 125.55 , 123.65 , 120.37 , 120.17 , 118.63 (2C), 117.16 , 112.16 , 102.39 , 24.14 . HRMS (ESI): *m/z* $[M-H]^-$ calculated for $C_{25}H_{19}N_4O_3S^-$, 455.1183; found, 455.1180.

N-(4-(N-(3-cyano-4-(methyl(naphthalen-2-yl)amino)phenyl)sulfamoyl)phenyl)acetamide ***(20)***. According to general procedure 2, the yellow solid **20** was got from **45j** and 4-acetamidobenzenesulfonyl chloride (yield 65%). ^{1}H NMR (400 MHz, DMSO-d_6) δ 10.58 (s, 1H), 10.38 (s, 1H), 7.78 – 7.73 (m, 5H), 7.71 (d, J = 3.4 Hz, 1H), 7.69 (d, J = 2.4 Hz, 1H), 7.44 – 7.37 (m, 3H), 7.34 – 7.25 (m, 2H), 7.11 (d, J = 2.3 Hz, 1H), 6.88 (dd, J = 9.0, 2.4 Hz, 1H), 3.32 (s, 3H), 2.09 (s, 3H).^{13}C NMR (101 MHz, DMSO-d_6) δ 169.10 , 147.16 , 146.12 , 143.48 , 135.12 , 134.15 , 132.50 , 128.71 , 128.15 , 128.07 (2C), 127.99 , 127.36 , 126.53 , 126.43 (2C), 124.62 , 123.36 , 118.68 (3C), 116.70 , 110.52 , 110.19 , 40.50 , 24.15 .HRMS (ESI): *m/z* $[M-H]^-$ calculated for $C_{26}H_{21}N_4O_3S^-$, 469.1340;

found, 469.1350.

N-(4-(N-(3-cyano-4-phenoxyphenyl)sulfamoyl)phenyl)acetamide ***(21)***. Starting with 4-acetamidobenzenesulfonyl chloride and **47a**, **21** was obtained as a white solid by using general procedure 2 (yield 69%). ^{1}H NMR (400 MHz, DMSO-d_6) δ 10.44 (s, 1H), 10.34 (s, 1H), 7.80 – 7.65 (m, 4H), 7.45 (d, J = 2.7 Hz, 1H), 7.45 – 7.39 (m, 2H), 7.33 (dd, J = 9.1, 2.7 Hz, 1H), 7.25 – 7.19 (m, 1H), 7.10 – 7.03 (m, 2H), 6.92 (d, J = 9.1 Hz, 1H), 2.07 (s, 3H).^{13}C NMR (101 MHz, DMSO-d_6) δ 169.09 , 155.27 , 155.02 , 143.41 , 133.61 , 132.38 , 130.34 (2C), 128.02 (2C), 127.59 , 124.99 , 124.79 , 119.29 , 118.98 (2C), 118.66 (2C), 115.35 , 103.52 , 24.14 .HRMS (ESI): *m/z* $[M-H]^-$ calculated for $C_{21}H_{16}N_3O_4S^-$, 406.0867; found, 406.0861.

N-(4-(N-(3-cyano-4-(4-fluorophenoxy)phenyl)sulfamoyl)phenyl)acetamide ***(22)***. According to general procedure 2, the white solid **22** was got from **47b** and 4-acetamidobenzenesulfonyl chloride (yield 71%). ^{1}H NMR (400 MHz, DMSO-d_6) δ 10.42 (s, 1H), 10.34 (s, 1H), 7.78 – 7.65 (m, 4H), 7.45 (d, J = 2.7 Hz, 1H), 7.31 (dd, J = 9.1, 2.7 Hz, 1H), 7.29 – 7.22 (m, 2H), 7.19 – 7.11 (m, 2H), 6.88 (d, J = 9.1 Hz, 1H), 2.07 (s, 3H).^{13}C NMR (101 MHz, DMSO-d_6) δ 169.09 , 158.97(d, J = 241.2 Hz) , 155.44 , 151.12 , 143.40 , 133.46 , 132.40 , 128.01 (2C), 127.58 , 125.03 , 121.29 (d, J = 8.6 Hz, 2C), 118.67 (2C), 118.58 , 116.91 (d, J = 23.6 Hz, 2C), 115.33 , 103.08 , 24.13 .HRMS (ESI): *m/z* $[M-H]^-$ calculated for $C_{21}H_{15}FN_3O_4S^-$, 424.0773; found, 424.0780.

N-(4-(N-(4-(4-chlorophenoxy)-3-cyanophenyl)sulfamoyl)phenyl)acetamide ***(23)***. Starting with 4-acetamidobenzenesulfonyl chloride and **47c**, **23** was obtained as a white solid by

using general procedure 2 (yield 77%). ^{1}H NMR (400 MHz, DMSO-d_6) δ 10.47 (s, 1H), 10.34 (s, 1H), 7.78 – 7.66 (m, 4H), 7.50 – 7.41 (m, 3H), 7.33 (dd, J = 9.0, 2.7 Hz, 1H), 7.13 – 7.05 (m, 2H), 6.97 (d, J = 9.0 Hz, 1H), 2.07 (s, 3H).^{13}C NMR (101 MHz, DMSO-d_6) δ 169.09 , 154.51 , 154.24 , 143.43 , 133.99 , 132.37 , 130.18 (2C), 128.67, 128.02 (2C), 127.44 , 124.89 , 120.74 (2C), 119.60 , 118.68 (2C), 115.21 , 103.74 , 24.14.HRMS (ESI): *m/z* [M-H]$^-$ calculated for $C_{21}H_{15}ClN_3O_4S^-$, 440.0477; found, 440.0477.

N-(4-(N-(3-cyano-4-(4-cyanophenoxy)phenyl)sulfamoyl)phenyl)acetamide ***(24)***.

According to general procedure 2, the white solid **24** was got from **47d** and 4-acetamidobenzenesulfonyl chloride (yield 68%). ^{1}H NMR (400 MHz, DMSO-d_6) δ 10.59 (s, 1H), 10.35 (s, 1H), 7.94 – 7.84 (m, 2H), 7.79 – 7.68 (m, 4H), 7.50 (d, J = 2.7 Hz, 1H), 7.39 (dd, J = 9.0, 2.7 Hz, 1H), 7.24 – 7.15 (m, 3H), 2.07 (s, 3H).^{13}C NMR (101 MHz, DMSO-d_6) δ 169.09 , 159.58 , 152.41 , 143.46 , 135.23 , 134.87 (2C), 132.34 , 128.03 (2C), 127.08 , 124.58 , 121.68 , 118.69 (2C), 118.63 (2C), 118.41 , 114.88 , 106.63 , 105.05 , 24.13 .HRMS (ESI): *m/z* [M-H]$^-$ calculated for $C_{22}H_{15}N_4O_4S^-$, 431.0819; found, 431.0826.

N-(4-(N-(4-(4-chloro-3-fluorophenoxy)-3-cyanophenyl)sulfamoyl)phenyl)acetamide ***(25)***.

Starting with 4-acetamidobenzenesulfonyl chloride and **47e**, **25** was obtained as a white solid by using general procedure 2 (yield 72%).^{1}H NMR (400 MHz, DMSO-d_6) δ 10.51 (s, 1H), 10.34 (s, 1H), 7.78 – 7.67 (m, 4H), 7.61 (t, J = 8.7 Hz, 1H), 7.47 (d, J = 2.6 Hz, 1H), 7.37 – 7.28 (m, 2H), 7.08 (d, J = 9.1 Hz, 1H), 6.98 – 6.91 (m, 1H), 2.07 (s, 3H).^{13}C

NMR (126 MHz, DMSO-d_6) δ 169.06 , 157.67 (d, J = 248.3 Hz), 155.25 (d, J = 9.9 Hz), 153.75 , 143.43 , 134.43 , 132.36 , 131.57 , 128.00 (2C), 127.24 , 124.72 , 120.06 , 118.67 (2C), 116.01 (d, J = 3.2 Hz), 115.23 (d, J = 17.7 Hz), 115.05 , 108.40 (d, J = 24.3 Hz), 103.99 , 24.11 .HRMS (ESI): *m/z* [M-H]$^-$ calculated for $C_{21}H_{14}ClFN_3O_4S^-$, 458.0383; found, 458.0381.

N-(4-(N-(3-cyano-4-(3,4-dichlorophenoxy)phenyl)sulfamoyl)phenyl)acetamide ***(26)***. According to general procedure 2, the white solid **26** was got from **47f** and 4-acetamidobenzenesulfonyl chloride (yield 81%). ^{1}H NMR (400 MHz, DMSO-d_6) δ 10.43 (br s, 1H), 10.33 (s, 1H), 7.77 – 7.68 (m, 4H), 7.65 (dd, J = 8.9, 2.0 Hz, 1H), 7.48 – 7.43 (m, 2H), 7.33 (dd, J = 9.0, 2.3 Hz, 1H), 7.11 – 7.03 (m, 2H), 2.07 (s, 3H).^{13}C NMR (126 MHz, DMSO-d_6) δ 169.06 , 154.80 , 153.73 , 143.38 , 134.56 , 132.44 , 132.30 , 131.80 , 127.99 (2C), 127.28 , 126.89 , 124.72 , 121.06 , 120.03 , 119.23 , 118.66 (2C), 115.08 , 103.97 , 24.12 .HRMS (ESI): *m/z* [M-H]$^-$ calculated for $C_{21}H_{14}Cl_2N_3O_4S^-$, 474.0088; found, 474.0085.

N-(4-(N-(4-(4-chloro-3-cyanophenoxy)-3-cyanophenyl)sulfamoyl)phenyl)acetamide ***(27)***. Starting with 4-acetamidobenzenesulfonyl chloride and **47g**, **27** was obtained as a white solid by using general procedure 2 (yield 76%). ^{1}H NMR (400 MHz, DMSO-d_6) δ 10.54 (s, 1H), 10.33 (s, 1H), 7.85 (d, J = 2.9 Hz, 1H), 7.78 – 7.67 (m, 5H), 7.50 – 7.44 (m, 2H), 7.33 (dd, J = 9.1, 2.7 Hz, 1H), 7.09 (d, J = 9.1 Hz, 1H), 2.07 (s, 3H).^{13}C NMR (101 MHz, DMSO-d_6) δ 169.09 , 154.35 , 153.54 , 143.44 , 134.59 , 132.38 , 131.93 , 131.02 , 128.01 (2C), 127.10 , 125.67 , 124.75 , 124.64 , 120.06 , 118.71 (2C), 115.22 , 115.04 ,

113.45 , 104.07 , 24.13 .HRMS (ESI): *m/z* [M-H]$^-$ calculated for $C_{22}H_{14}ClN_4O_4S^-$, 465.0430; found, 465.0432.

*N-(4-(N-(4-(4-chloro-3-methylphenoxy)-3-cyanophenyl)sulfamoyl)phenyl)acetamide (**28**).* According to general procedure 2, the white solid **28** was got from **47h** and 4-acetamidobenzenesulfonyl chloride (yield 77%).^{1}H NMR (400 MHz, DMSO-d_6) δ 10.45 (br s, 1H), 10.33 (s, 1H), 7.76 – 7.64 (m, 4H), 7.47 – 7.41 (m, 2H), 7.31 (dd, J = 9.1, 2.6 Hz, 1H), 7.11 (d, J = 2.7 Hz, 1H), 6.96 (d, J = 9.1 Hz, 1H), 6.92 (dd, J = 8.7, 2.8 Hz, 1H), 2.30 (s, 3H), 2.07 (s, 3H). ^{13}C NMR (126 MHz, DMSO-d_6) δ 169.06 , 154.58 , 153.98 , 143.36 , 137.79 , 133.94 , 132.43 , 130.34 , 128.93 , 127.99 (2C), 127.48 , 124.83 , 121.57 , 119.47 , 118.64 (2C), 118.07 , 115.23 , 103.55 , 24.12 , 19.62 .HRMS (ESI): *m/z* [M-H]$^-$ calculated for $C_{22}H_{17}ClN_3O_4S^-$, 454.0634; found, 454.0627.

*N-(4-(N-(4-(4-chloro-3-(trifluoromethyl)phenoxy)-3-cyanophenyl)sulfamoyl)phenyl)acetamide (**29**).* Starting with 4-acetamidobenzenesulfonyl chloride and **47i**, **29** was obtained as a white solid by using general procedure 2 (yield 72%). ^{1}H NMR (400 MHz, DMSO-d_6) δ 10.52 (s, 1H), 10.33 (s, 1H), 7.77 – 7.68 (m, 5H), 7.60 (d, J = 2.9 Hz, 1H), 7.48 (d, J = 2.7 Hz, 1H), 7.39 (dd, J = 8.8, 2.9 Hz, 1H), 7.33 (dd, J = 9.1, 2.7 Hz, 1H), 7.09 (d, J = 9.1 Hz, 1H), 2.07 (s, 3H).^{13}C NMR (126 MHz, DMSO-d_6) δ 169.04 , 154.29 , 153.67 , 143.42 , 134.50 , 133.60 , 132.32 , 128.24 (q, J = 31.5 Hz) , 127.99 (2C), 127.21 , 126.05 , 124.74 , 124.27 , 122.20 (q, J = 273.9 Hz) , 119.98 , 118.71 (q, J = 5.5 Hz), 118.65 (2C), 115.02 , 104.04 , 24.10 .HRMS (ESI): *m/z* [M-H]$^-$ calculated for $C_{22}H_{14}ClF_3N_3O_4S^-$, 508.0351; found, 508.0354.

*N-(4-(N-(4-(4-chloro-3-methoxyphenoxy)-3-cyanophenyl)sulfamoyl)phenyl)acetamide (**30**).* According to general procedure 2, the white solid **30** was got from **47j** and 4-acetamidobenzenesulfonyl chloride (yield 85%). ^{1}H NMR (400 MHz, DMSO-d_6) δ 10.43 (s, 1H), 10.33 (s, 1H), 7.76 – 7.67 (m, 4H), 7.48 – 7.39 (m, 2H), 7.31 (dd, J = 9.1, 2.7 Hz, 1H), 7.01 – 6.91 (m, 2H), 6.60 (dd, J = 8.7, 2.6 Hz, 1H), 3.82 (s, 3H), 2.07 (s, 3H).^{13}C NMR (126 MHz, DMSO-d_6) δ 169.07 , 155.76 , 154.96 , 154.74 , 143.39 , 133.74 , 132.36 , 130.64 , 128.00 (2C), 127.48 , 124.87 , 119.17 , 118.64 (2C), 117.00 , 115.26 , 111.42 , 104.92 , 103.35 , 56.40 , 24.11 .HRMS (ESI): *m/z* [M-H]$^-$ calculated for $C_{22}H_{17}ClN_3O_5S^-$, 470.0583; found, 470.0579.

*N-(4-(N-(4-(3-benzyl-4-chlorophenoxy)-3-cyanophenyl)sulfamoyl)phenyl)acetamide (**31**).* Starting with 4-acetamidobenzenesulfonyl chloride and **47k**, **31** was obtained as a white solid by using general procedure 2 (yield 73%).^{1}H NMR (400 MHz, DMSO-d_6) δ 10.46 (s, 1H), 10.33 (s, 1H), 7.78 – 7.63 (m, 4H), 7.46 (d, J = 8.7 Hz, 1H), 7.43 (d, J = 2.6 Hz, 1H), 7.31 (dd, J = 9.1, 2.7 Hz, 1H), 7.29 – 7.23 (m, 2H), 7.23 – 7.14 (m, 3H), 7.12 (d, J = 2.9 Hz, 1H), 6.99 – 6.92 (m, 2H), 4.04 (s, 2H), 2.06 (s, 3H). ^{13}C NMR (126 MHz, DMSO-d_6) δ 169.03 , 154.46 , 154.13 , 143.39 , 140.61 , 138.81 , 133.87 , 132.35 , 130.92 , 128.74 , 128.59 (2C), 128.41 (2C), 127.98 (2C), 127.36 , 126.24 , 124.79 , 121.74 , 119.43 , 118.63 (2C), 118.47 , 115.17 , 103.57 , 38.34 , 24.10 . HRMS (ESI): *m/z* [M-H]$^-$ calculated for $C_{28}H_{21}ClN_3O_4S^-$, 530.0947; found, 530.0952.

*N-(4-(N-(4-((6-chloro-[1,1'-biphenyl]-3-yl)oxy)-3-cyanophenyl)sulfamoyl)phenyl)acetamide (**31a**).* According to general procedure 2, the white solid **31a** was got from **47l** and

4-acetamidobenzenesulfonyl chloride (yield 67%).^{1}H NMR (400 MHz, DMSO-d_6) δ 10.47 (s, 1H), 10.33 (s, 1H), 7.76 – 7.66 (m, 4H), 7.60 (d, J = 8.7 Hz, 1H), 7.51 – 7.38 (m, 6H), 7.33 (dd, J = 9.1, 2.6 Hz, 1H), 7.17 – 7.04 (m, 3H), 2.07 (s, 3H). ^{13}C NMR (126 MHz, DMSO-d_6) δ 169.03 , 154.41 , 154.20 , 143.38 , 141.51 , 137.81 , 133.95 , 132.35 , 131.55 , 129.12 (2C), 128.23 (2C), 128.07 , 127.97 (2C), 127.37 , 126.90 , 124.77 , 121.72 , 119.63 , 119.50 , 118.64 (2C), 115.22 , 103.71 , 24.11 . HRMS (ESI): *m/z* [M-H]$^-$ calculated for $C_{27}H_{19}ClN_3O_4S^-$, 516.0790; found, 516.0797.

*N-(4-(N-(3-cyano-4-(4-fluoro-3-(trifluoromethyl)phenoxy)phenyl)sulfamoyl)phenyl)acetamide (**32**).* Starting with 4-acetamidobenzenesulfonyl chloride and **47m**, **32** was obtained as a white solid by using general procedure 2 (yield 72%). ^{1}H NMR (400 MHz, DMSO-d_6) δ 10.48 (s, 1H), 10.33 (s, 1H), 7.78 – 7.67 (m, 4H), 7.60 – 7.53 (m, 2H), 7.52 – 7.45 (m, 2H), 7.32 (dd, J = 9.1, 2.7 Hz, 1H), 6.99 (d, J = 9.1 Hz, 1H), 2.07 (s, 3H).^{13}C NMR (126 MHz, DMSO-d_6) δ 169.07 , 155.57 (d, J = 251.8 Hz) , 154.61, 151.11 (d, J = 2.3 Hz) , 143.44 , 134.06 , 132.40 , 128.01 (2C), 127.35 , 125.94 (d, J = 8.8 Hz) , 124.89 , 122.00（q, J = 273.4 Hz）, 119.23 (d, J = 22.6 Hz) , 119.05 , 118.69 (2C), 118.42 (q, J = 3.9 Hz) , 118.02 (qd, J = 33.2 Hz, J = 14.2 Hz) , 115.17 , 103.51 , 24.10 .HRMS (ESI): *m/z* [M-H]$^-$ calculated for $C_{22}H_{14}F_4N_3O_4S^-$, 492.0647; found, 492.0636.

*N-(4-(N-(3-cyano-4-(4-cyano-3-(trifluoromethyl)phenoxy)phenyl)sulfamoyl)phenyl)acetamide (**33**).* According to general procedure 2, the white solid **33** was got from **47n** and 4-acetamidobenzenesulfonyl chloride (yield 75%). ^{1}H NMR (400 MHz, DMSO-d_6) δ 10.67 (br s, 1H), 10.34 (s, 1H), 8.17 (d, J = 8.6 Hz, 1H), 7.79 – 7.65 (m, 5H), 7.53 (d, J =

2.5 Hz, 1H), 7.45 (dd, *J* = 8.6, 2.0 Hz, 1H), 7.40 (dd, *J* = 9.0, 2.6 Hz, 1H), 7.27 (d, *J* = 9.0 Hz, 1H), 2.07 (s, 3H).^{13}C NMR (126 MHz, DMSO-d_6) δ 169.07 , 159.59 , 151.68 , 143.49 , 138.04 , 135.80 , 133.34 (q, *J* = 32.5 Hz), 132.38 , 128.02 (2C), 126.89 , 124.49 , 121.97 (q, *J* = 274.7 Hz), 121.75 , 121.62 , 118.69 (2C), 117.09 (q, *J* = 4.5 Hz), 115.21 , 114.75 , 105.23 , 103.54 , 24.11 .HRMS (ESI): *m/z* [M-H]$^-$ calculated for $C_{23}H_{14}F_3N_4O_4S^-$, 499.0693; found, 499.0702.

N-(4-(4-chloro-3-(trifluoromethyl)phenoxy)-3-cyanophenyl)benzenesulfonamide ***(34)***. Starting with benzenesulfonyl chloride and **47i**, **34** was obtained as colorless oil by using general procedure 2 (yield 86%). ^{1}H NMR (400 MHz, DMSO-d_6) δ 10.66 (s, 1H), 7.82 – 7.76 (m, 2H), 7.74 (d, *J* = 8.8 Hz, 1H), 7.67 – 7.61 (m, 1H), 7.60 – 7.54 (m, 3H), 7.51 (d, *J* = 2.7 Hz, 1H), 7.38 (td, *J* = 9.3, 2.8 Hz, 2H), 7.09 (d, *J* = 9.1 Hz, 1H).^{13}C NMR (126 MHz, DMSO-d_6) δ 154.26 , 153.83 , 138.94 , 134.33 , 133.59 , 133.24 , 129.41 (2C), 128.28 (q, *J* = 31.5 Hz), 127.34 , 126.67 (2C), 126.13 , 124.91 , 124.27 , 122.19 (q, *J* = 273.4 Hz), 119.98 , 118.66 (q, *J* = 5.6 Hz), 114.96 , 104.13 .HRMS (ESI): *m/z* [M-H]$^-$ calculated for $C_{20}H_{11}ClF_3N_2O_3S^-$, 451.0136; found, 451.0140.

N-(4-(4-chloro-3-(trifluoromethyl)phenoxy)-3-cyanophenyl)-4-methylbenzenesulfonamide ***(35)***. According to general procedure 2, the white solid **35** was got from **47i** and 4-methylbenzenesulfonyl chloride (yield 86%). ^{1}H NMR (400 MHz, DMSO-d_6) δ 10.59 (s, 1H), 7.73 (d, *J* = 8.8 Hz, 1H), 7.67 (d, *J* = 8.3 Hz, 2H), 7.56 (d, *J* = 2.9 Hz, 1H), 7.50 (d, *J* = 2.7 Hz, 1H), 7.44 – 7.30 (m, 4H), 7.09 (d, *J* = 9.1 Hz, 1H), 2.33 (s, 3H).^{13}C NMR (126 MHz, DMSO-d_6) δ 154.30 , 153.67 , 143.67 , 136.12 , 134.51 , 133.59 , 129.83 (2C),

128.27 (q, *J* = 31.4 Hz), 127.12 , 126.72 (2C), 126.09 , 124.66 , 124.24 , 122.19 (q, *J* = 273.4 Hz), 120.02 , 118.60 (q, *J* = 5.2 Hz), 114.99 , 104.14 , 20.93 .HRMS (ESI): *m/z* [M--H]$^-$ calculated for $C_{21}H_{13}ClF_3N_2O_3S^-$, 465.0293; found, 465.0294.

*N-(4-(4-chloro-3-(trifluoromethyl)phenoxy)-3-cyanophenyl)-4-nitrobenzenesulfonamide (**36**)*. Starting with 4-nitrobenzenesulfonyl chloride and **47i**, **36** was obtained as a yellow solid by using general procedure 2 (yield 84%). ^{1}H NMR (400 MHz, DMSO-d_6) δ 10.94 (s, 1H), 8.39 (d, *J* = 8.9 Hz, 2H), 8.02 (d, *J* = 8.9 Hz, 2H), 7.77 (d, *J* = 8.8 Hz, 1H), 7.62 (d, *J* = 2.9 Hz, 1H), 7.56 (d, *J* = 2.6 Hz, 1H), 7.43 (dd, *J* = 8.8, 2.8 Hz, 1H), 7.35 (dd, *J* = 9.1, 2.7 Hz, 1H), 7.10 (d, *J* = 9.1 Hz, 1H). ^{13}C NMR (126 MHz, DMSO-d_6) δ 154.50 , 154.07 , 149.99 , 144.25 , 133.63 , 133.34 , 128.32 (2C), 128.27 (q, *J* = 31.7 Hz), 128.10 , 126.26 , 125.79 , 124.77 (2C), 124.53 , 122.18 (q, *J* = 273.4 Hz), 119.86 , 118.91 (d, *J* = 5.1 Hz), 114.91 , 104.19 . HRMS (ESI): *m/z* [M-H]$^-$ calculated for $C_{20}H_{10}ClF_3N_3O_5S^-$, 495.9987; found, 495.9979.

*4-amino-N-(4-(4-chloro-3-(trifluoromethyl)phenoxy)-3-cyanophenyl)benzenesulfonamide (**37**)*. According to step b in general procedure 1, the white solid **37** was got from **36** (yield 83%). ^{1}H NMR (400 MHz, DMSO-d_6) δ 10.22 (s, 1H), 7.75 (d, *J* = 8.8 Hz, 1H), 7.60 (d, *J* = 2.9 Hz, 1H), 7.43 (d, *J* = 2.7 Hz, 1H), 7.42 – 7.38 (m, 2H), 7.38 – 7.32 (m, 2H), 7.10 (d, *J* = 9.1 Hz, 1H), 6.59 – 6.53 (m, 2H), 6.07 (s, 2H).^{13}C NMR (126 MHz, DMSO-d_6) δ 154.48 , 153.21 , 153.08 , 135.33 , 133.61 , 128.81 (2C), 128.24 (q, *J* = 31.5 Hz), 126.59 , 125.94 , 124.08 , 123.94 , 123.47 , 122.23 (q, *J* = 273.3 Hz), 120.11 , 118.57 (q, *J* = 5.3 Hz), 115.15 , 112.67 (2C), 103.99 .HRMS (ESI): *m/z* [M-H]$^-$ calculated

for $C_{20}H_{12}ClF_3N_3O_3S^-$, 466.0245; found, 466.0247.

*N-(4-(N-(4-(4-chloro-3-(trifluoromethyl)phenoxy)-3-cyanophenyl)sulfamoyl)phenyl)-N-methylacetamide (**38**).* Starting with **48a** and **47i**, **38** was obtained as a colorless oil by using general procedure 2 (yield 76%). ^{1}H NMR (400 MHz, DMSO-d_6) δ 10.67 (s, 1H), 7.80 (d, J = 8.5 Hz, 2H), 7.76 (dd, J = 8.9, 3.1 Hz, 1H), 7.60 (d, J = 2.8 Hz, 1H), 7.54 (d, J = 8.5 Hz, 2H), 7.50 (d, J = 2.4 Hz, 1H), 7.44 – 7.34 (m, 2H), 7.10 (d, J = 9.1 Hz, 1H), 3.36 (s, 3H), 3.20 (s, 3H).^{13}C NMR (126 MHz, DMSO-d_6) δ 169.22 , 154.25 , 153.99 , 148.16 , 136.61 , 134.19 , 133.65 , 128.28 (q, J = 31.4 Hz), 127.85 (2C), 127.57 , 127.24 , 126.18 , 125.12 , 124.36 , 122.22 (q, J = 273.7 Hz) ,120.00 (2C), 118.76 (q, J = 5.0 Hz) , 114.98 , 104.15 , 36.80 , 22.48 .HRMS (ESI): *m/z* [M-H]$^-$ calculated for $C_{23}H_{16}ClF_3N_3O_4S^-$, 522.0508; found, 522.0514.

*N-(4-(N-(4-(4-chloro-3-(trifluoromethyl)phenoxy)-3-cyanophenyl)sulfamoyl)benzyl)acetamide (**39**).* According to general procedure 2, the white solid **39** was got from **47i** and **48b** (yield 73%). ^{1}H NMR (400 MHz, Chloroform-*d*) δ 8.76 (s, 1H), 7.62 (d, J = 8.4 Hz, 2H), 7.51 (d, J = 8.7 Hz, 1H), 7.42 – 7.36 (m, 2H), 7.34 – 7.29 (m, 3H), 7.13 (dd, J = 8.7, 2.9 Hz, 1H), 6.88 – 6.75 (m, 1H), 6.58 – 6.41 (m, 1H), 4.48 (d, J = 6.2 Hz, 2H), 2.13 (s, 3H).^{13}C NMR (126 MHz, DMSO-d_6) δ 169.44 , 154.25 , 153.73 , 145.41 , 137.41 , 134.43 , 133.63 , 128.27 (q, J = 31.6 Hz), 127.87 (d, J = 8.6 Hz, 2C), 127.03 (d, J = 6.6 Hz), 126.78 (2C), 126.13 , 124.54 (d, J = 11.1 Hz), 124.36 (d, J = 8.9 Hz), 122.23 (q, J = 273.3 Hz), 119.94 , 118.82 , 115.04 , 104.08 , 41.66 , 22.50 .HRMS (ESI): *m/z* [M-H]$^-$ calculated for $C_{23}H_{16}ClF_3N_3O_4S^-$, 522.0508; found, 522.0515.

*N-(4-(N-(4-(4-chloro-3-(trifluoromethyl)phenoxy)-3-cyanophenyl)sulfamoyl)phenyl)morpholine-4-carboxamide (**40**).* Starting with **48c** and **47i**, **40** was obtained as a white solid by using general procedure 2 (yield 73%). ^{1}H NMR (400 MHz, DMSO-d_6) δ 10.47 (s, 1H), 8.97 (s, 1H), 7.75 (d, J = 8.8 Hz, 1H), 7.68 – 7.62 (m, 4H), 7.61 (d, J = 2.9 Hz, 1H), 7.48 (d, J = 2.7 Hz, 1H), 7.38 (dd, J = 8.8, 2.9 Hz, 1H), 7.35 (dd, J = 9.1, 2.7 Hz, 1H), 7.09 (d, J = 9.1 Hz, 1H), 3.63 – 3.57 (m, 4H), 3.47 – 3.39 (m, 4H).^{13}C NMR (126 MHz, DMSO-d_6) δ 154.45 , 154.33 , 153.59 , 145.08 , 134.68 , 133.62 , 130.80 , 128.26 (q, J = 31.6 Hz), 127.71 (2C), 127.08 , 126.06 , 124.55 , 124.25 , 122.22 (q, J = 273.3 Hz), 120.00 , 118.74 (q, J = 5.4 Hz), 118.67 (2C), 115.07 , 104.04 , 65.94 (2C), 44.20 (2C).HRMS (ESI): *m/z* [M-H]$^-$ calculated for $C_{25}H_{19}ClF_3N_4O_5S^-$, 579.0722; found, 579.0734.

*4-(N-(4-(4-chloro-3-(trifluoromethyl)phenoxy)-3-cyanophenyl)sulfamoyl)benzoic acid (**41**).* According to general procedure 2, the white solid **41** was got from **47i** and 4-(chlorosulfonyl)benzoic acid (yield 76%). ^{1}H NMR (400 MHz, DMSO-d_6) δ 13.46 (br s, 1H), 10.82 (br s, 1H), 8.10 (d, J = 8.5 Hz, 2H), 7.88 (d, J = 8.5 Hz, 2H), 7.74 (d, J = 8.8 Hz, 1H), 7.59 (d, J = 2.9 Hz, 1H), 7.53 (d, J = 2.7 Hz, 1H), 7.41 (dd, J = 8.8, 2.8 Hz, 1H), 7.34 (dd, J = 9.1, 2.7 Hz, 1H), 7.09 (d, J = 9.1 Hz, 1H).^{13}C NMR (126 MHz, DMSO-d_6) δ 166.02 , 154.18 (2C), 142.47 , 134.89 , 133.85 , 133.62 , 130.28 (2C), 128.28 (q, J = 31.7 Hz), 127.76 , 127.02 (2C), 126.19 , 125.43 , 124.42 , 122.20 (d, J = 273.5 Hz), 119.93 , 118.80 (d, J = 5.4 Hz), 114.96 , 104.17 .HRMS (ESI): *m/z* [M-H]$^-$ calculated for $C_{21}H_{11}ClF_3N_2O_5S^-$, 495.0035; found, 495.0044.

*N-(4-(4-chloro-3-(trifluoromethyl)phenoxy)-3-cyanophenyl)-4-morpholinobenzenesulfonamide (**42**).* To a solution of **49** (0.1 mM) in DMSO was added morpholine (0.5mM), and the mixture was heated at 120 ℃ for 10h. The reaction was quenched with water, extracted with DCM (×3), washed the brine (×3), dried with anhydrous $MgSO_4$, filtered, and evaporated in vacuo. The residue was purified by column chromatography (DCM/MeOH=50:1) to afford **42** (yield 45%). ^{1}H NMR (400 MHz, DMSO-d_6) δ 10.42 (s, 1H), 7.73 (d, J = 8.8 Hz, 1H), 7.59 (d, J = 8.9 Hz, 2H), 7.57 (d, J = 2.6 Hz, 1H), 7.49 (d, J = 2.3 Hz, 1H), 7.41 – 7.33 (m, 2H), 7.10 (d, J = 9.1 Hz, 1H), 7.00 (d, J = 8.9 Hz, 2H), 3.75 – 3.64 (m, 4H), 3.31 – 3.18 (s, 4H).^{13}C NMR (126 MHz, DMSO-d_6) δ 154.39 , 153.57 , 153.27 , 135.02 , 133.57 , 128.36 (2C), 128.26 (q, J = 31.6 Hz) , 126.73 , 126.65 , 126.00 , 124.11 , 124.06 , 122.19 (q, J = 273.9 Hz) , 120.10 , 118.51 (q, J = 5.2 Hz), 115.07 , 113.29 (2C), 104.09 , 65.75 (2C), 46.58 (2C).HRMS (ESI): *m/z* $[M+Na]^+$ calculated for $C_{24}H_{19}ClF_3N_3NaO_4S^+$, 560.0629; found, 560.0631.

*N-(4-(4-chloro-3-(trifluoromethyl)phenoxy)-3-cyanophenyl)-4-(piperazin-1-yl)benzenesulfonamide (**43**).* According to the preparation of **42**, the white solid **43** was got from **49** and piperazine (yield 52%). ^{1}H NMR (400 MHz, DMSO-d_6) δ 7.74 (d, J = 8.8 Hz, 1H), 7.61 (d, J = 9.0 Hz, 2H), 7.57 (d, J = 2.9 Hz, 1H), 7.50 (d, J = 2.7 Hz, 1H), 7.41 – 7.35 (m, 2H), 7.09 (d, J = 9.1 Hz, 1H), 7.04 (d, J = 9.0 Hz, 2H), 3.52 – 3.40 (m, 4H), 3.14 – 3.00 (m, 4H).^{13}C NMR (126 MHz, DMSO-d_6) δ 154.46 , 153.09 , 152.79 , 135.41 , 133.63 , 128.42 (2C), 128.24 (q, J = 31.6 Hz) , 127.55 , 126.83 , 125.96 , 124.18 , 124.10 ,

122.23 (q, *J* = 273.8 Hz), 120.14 , 118.51 (q, *J* = 5.1 Hz) , 115.15 , 113.98 (2C), 104.04 , 44.52 (2C), 42.86 (2C).HRMS (ESI): *m/z* $[M+H]^+$ calculated for $C_{24}H_{21}ClF_3N_4O_3S^+$, 537.0970; found, 537.0970.

ASSOCIATED CONTENTS

Supporting Information

The materials are available free of charge via the Internet at http://pubs.acs.org.

Protein Expression and Purification, Docking Protocols, Figure S1, Table S1, Figure S2, Table S2, Figures S3-S4, Table S3, Chemistry of intermediates and **13b**-**17b**, **52**-**55**. (PDF)

Molecular formula strings (CSV)

Accession Codes

Coordinates for crystal structures of Lp-PLA2 in complex with compounds **10**, **11**, **14a** and **41** have been deposited in Protein Data Bank (PDB) with accession codes 5YE8 (**10**), 5YE7 (**11**), 5YE9 (**14a**) and 5YEA (**41**), respectively. We will release the atomic coordinates and experimental data upon article publication.

AUTHOR INFORMATION

Corresponding authors

*(J.S.) Phone: +86-21-20231969. E-mail: jhshen@ simm.ac.cn

*(Y.X.) Phone: +86-21-50801267. E-mail: ycxu@simm.ac.cn

Author contribution

The manuscript was written through contributions of all authors. All authors have given approval to the final version of the manuscript. ‡These authors contributed equally.

Funding Sources

This work was supported by the National Key R&D Program of China (No. 2017YFB0202604 and 2016YFA0502301) and the National Natural Science Foundation of China (No. 81422047, No. 81661148046, No. 81602963 and No. 81673302).

Notes

The authors declare no competing financial interest.

ABBREVIATIONS

Lp-PLA2, lipoprotein-associated phospholipase A2; MW, molecular weight; LE, ligand efficiency; rhLp-PLA2, recombinant human Lp-PLA2; IC_{50}, half maximal inhibitory concentration; H-bond, hydrogen bond; SD-rats, Sprague-Dawley rats; HCl, hydrochloric acid; DCM, dichloromethane; PE, petroleum ether (boiling range: 60-90°C); EA and EtOAc, ethyl acetate; DMSO, dimethylsulfoxide; THF, tetrahydrofuran; DMF, *N*,*N*-dimethyl formamide; rt, room temperature.

REFERENCES

1. Schaloske, R. H.; Dennis, E. A. The phospholipase A2 superfamily and its group numbering system. *Biochim. Biophys. Acta* **2006,** *1761*, 1246-1259.

2. (a) Samanta, U.; Bahnson, B. J. Crystal structure of human plasma platelet-activating factor acetylhydrolase: structural implication to lipoprotein binding and catalysis. *J. Biol. Chem.* **2008,** *283*, 31617-31624; (b) Liu, Q.; Chen, X.; Chen, W.; Yuan, X.; Su, H.; Shen, J.; Xu, Y. Structural and thermodynamic characterization of protein-ligand interactions formed between lipoprotein-associated phospholipase A2 and inhibitors. *J. Med. Chem.* **2016,** *59*, 5115-5120.

3. Tjoelker, L. W.; Wilder, C.; Eberhardt, C.; Stafforini, D. M.; Dietsch, G.; Schimpf, B.; Hooper, S.; Le Trong, H.; Cousens, L. S.; Zimmerman, G. A.; Yamada, Y.; McIntyre, T. M.; Prescott, S. M.; Gray, P. W. Anti-inflammatory properties of a platelet-activating factor acetylhydrolase. *Nature* **1995,** *374*, 549-553.

4. Stremler, K. E.; Stafforini, D. M.; Prescott, S. M.; McIntyre, T. M. Human plasma platelet-activating factor acetylhydrolase. Oxidatively fragmented phospholipids as substrates. *J. Biol. Chem.* **1991,** *266*, 11095-11103.

5. Thompson, A.; Gao, P.; Orfei, L.; Watson, S.; Di Angelantonio, E.; Kaptoge, S.; Ballantyne, C.; Cannon, C. P.; Criqui, M.; Cushman, M.; Hofman, A.; Packard, C.; Thompson, S. G.; Collins, R.; Danesh, J. Lipoprotein-associated phospholipase A(2) and risk of coronary disease, stroke, and mortality: collaborative analysis of 32 prospective studies. *Lancet* **2010,** *375*, 1536-1544.

6. (a) Ikonomidis, I.; Kadoglou, N. N.; Tritakis, V.; Paraskevaidis, I.; Dimas, K.;

Trivilou, P.; Papadakis, I.; Tzortzis, S.; Triantafyllidi, H.; Parissis, J.; Anastasiou-Nana, M.; Lekakis, J. Association of Lp-PLA2 with digital reactive hyperemia, coronary flow reserve, carotid atherosclerosis and arterial stiffness in coronary artery disease. *Atherosclerosis* **2014,** *234*, 34-41; (b) Lin, J.; Zheng, H.; Cucchiara, B. L.; Li, J.; Zhao, X.; Liang, X.; Wang, C.; Li, H.; Mullen, M. T.; Johnston, S. C.; Wang, Y.; Wang, Y. Association of Lp-PLA2-A and early recurrence of vascular events after TIA and minor stroke. *Neurology* **2015,** *85*, 1585-1591.

7. Acharya, N. K.; Levin, E. C.; Clifford, P. M.; Han, M.; Tourtellotte, R.; Chamberlain, D.; Pollaro, M.; Coretti, N. J.; Kosciuk, M. C.; Nagele, E. P.; Demarshall, C.; Freeman, T.; Shi, Y.; Guan, C.; Macphee, C. H.; Wilensky, R. L.; Nagele, R. G. Diabetes and hypercholesterolemia increase blood-brain barrier permeability and brain amyloid deposition: beneficial effects of the LpPLA2 inhibitor darapladib. *J. Alzheimers Dis.* **2013,** *35*, 179-198.

8. Canning, P.; Kenny, B. A.; Prise, V.; Glenn, J.; Sarker, M. H.; Hudson, N.; Brandt, M.; Lopez, F. J.; Gale, D.; Luthert, P. J.; Adamson, P.; Turowski, P.; Stitt, A. W. Lipoprotein-associated phospholipase A2 (Lp-PLA2) as a therapeutic target to prevent retinal vasopermeability during diabetes. *Proc. Natl. Acad. Sci. U. S. A.* **2016,** *113*, 7213-7218.

9. Kokotou, M. G.; Limnios, D.; Nikolaou, A.; Psarra, A.; Kokotos, G. Inhibitors of phospholipase A2 and their therapeutic potential: an update on patents (2012-2016). *Expert Opin. Ther. Pat.* **2017,** *27*, 217-225.

10. Tew, D. G.; Boyd, H. F.; Ashman, S.; Theobald, C.; Leach, C. A. Mechanism of inhibition of LDL phospholipase A2 by monocyclic-beta-lactams. Burst kinetics and the effect of stereochemistry. *Biochemistry* **1998,** *37*, 10087-10093.

11. (a) Jeong, T. S.; Kim, M. J.; Yu, H.; Kim, K. S.; Choi, J. K.; Kim, S. S.; Lee, W. S. (E)-Phenyl- and -heteroaryl-substituted O-benzoyl-(or acyl)oximes as lipoprotein-associated phospholipase A2 inhibitors. *Bioorg. Med. Chem. Lett.* **2005,** *15*, 1525-1527; (b) Jeong, H. J.; Park, Y. D.; Park, H. Y.; Jeong, I. Y.; Jeong, T. S.; Lee, W. S. Potent inhibitors of lipoprotein-associated phospholipase A(2): benzaldehyde O-heterocycle-4-carbonyloxime. *Bioorg. Med. Chem. Lett.* **2006,** *16*, 5576-5579.

12. (a) Hu, Y.; Lin, E. C.; Pham, L. M.; Cajica, J.; Amantea, C. M.; Okerberg, E.; Brown, H. E.; Fraser, A.; Du, L.; Kohno, Y.; Ishiyama, J.; Kozarich, J. W.; Shreder, K. R. Amides of 4-hydroxy-8-methanesulfonylamino-quinoline-2-carboxylic acid as zinc-dependent inhibitors of Lp-PLA(2). *Bioorg. Med. Chem. Lett.* **2013,** *23*, 1553-1556; (b) Lin, E. C.; Hu, Y.; Amantea, C. M.; Pham, L. M.; Cajica, J.; Okerberg, E.; Brown, H. E.; Fraser, A.; Du, L.; Kohno, Y.; Ishiyama, J.; Kozarich, J. W.; Shreder, K. R. Amides of xanthurenic acid as zinc-dependent inhibitors of Lp-PLA(2). *Bioorg. Med. Chem. Lett.* **2012,** *22*, 868-871.

13. (a) Nagano, J. M.; Hsu, K. L.; Whitby, L. R.; Niphakis, M. J.; Speers, A. E.; Brown, S. J.; Spicer, T.; Fernandez-Vega, V.; Ferguson, J.; Hodder, P.; Srinivasan, P.; Gonzalez, T. D.; Rosen, H.; Bahnson, B. J.; Cravatt, B. F. Selective inhibitors and tailored activity probes for lipoprotein-associated phospholipase A(2). *Bioorg. Med. Chem. Lett.* **2013,** *23*,

839-843; (b) Grice, C. A.; Niphakis, M.; Jones, T. K. Lp-PLA2 Inhibitors WO Patent WO2017/059135 A1. 2017.

14. (a) Blackie, J. A.; Bloomer, J. C.; Brown, M. J.; Cheng, H. Y.; Hammond, B.; Hickey, D. M.; Ife, R. J.; Leach, C. A.; Lewis, V. A.; Macphee, C. H.; Milliner, K. J.; Moores, K. E.; Pinto, I. L.; Smith, S. A.; Stansfield, I. G.; Stanway, S. J.; Taylor, M. A.; Theobald, C. J. The identification of clinical candidate SB-480848: a potent inhibitor of lipoprotein-associated phospholipase A2. *Bioorg. Med. Chem. Lett.* **2003,** *13*, 1067-1070; (b) Jin, Y.; Wan, Z.; Zhang, Q. Compounds. US2012/0142717 A1. 2012; (c) Wan, Z.; Zhang, X.; Wang, J.; Peng, C.; Jin, Y.; Hu, Y. Compounds. WO2012/075917 A1. 2012; (d) Wan, Z.; Zhang, X.; Tong, Z.; Long, K.; Dowdell, S. E.; Manas, E. S.; Goodman, K. B. Tricyclic Compounds, Preparation Methods, and their Uses. WO2012/037782 A1. 2012; (e) Wan, Z.; Long, K.; Sang, Y.; Su, X. 2,3-Dihydroimidazo[1,2-c]pyrimidin-5(1H)-one Compounds Use as Lp-PLA2 Inhibitors. WO2013/013503 A1. 2013; (f) Wan, Z.; Long, K.; Zhang, X.; Yu, H. Bicyclic Pyrimidone Compounds. WO2013/014185 A1. 2013; (g) Wan, Z.; Zhang, X. Compounds. WO2014/114248 A1. 2014; (h) Wan, Z.; Zhang, X. Bicyclic Pyrimidone Compounds as Inhibitors of Lp-PLA2. WO2014/114249 A1. 2014; (i) Sang, Y.; Wan, Z.; Zhang, Q. 2,3-Dihydroimidazol[1,2-c]pyrimidin-5(1H)-one Based Lipoprotein-associated Phospholipase A2 (Lp-PLA2) Inhibitors. WO2014/114694 A1. 2014.

15. Chen, X.; Xu, W.; Wang, K.; Mo, M.; Zhang, W.; Du, L.; Yuan, X.; Xu, Y.; Wang, Y.; Shen, J. Discovery of a novel series of imidazo[1,2-a]pyrimidine derivatives as potent

and orally bioavailable lipoprotein-associated phospholipase A2 inhibitors. *J. Med. Chem.* **2015,** *58*, 8529-8541.

16. (a) White, H. D.; Held, C.; Stewart, R.; Tarka, E.; Brown, R.; Davies, R. Y.; Budaj, A.; Harrington, R. A.; Steg, P. G.; Ardissino, D.; Armstrong, P. W.; Avezum, A.; Aylward, P. E.; Bryce, A.; Chen, H.; Chen, M. F.; Corbalan, R.; Dalby, A. J.; Danchin, N.; De Winter, R. J.; Denchev, S.; Diaz, R.; Elisaf, M.; Flather, M. D.; Goudev, A. R.; Granger, C. B.; Grinfeld, L.; Hochman, J. S.; Husted, S.; Kim, H. S.; Koenig, W.; Linhart, A.; Lonn, E.; Lopez-Sendon, J.; Manolis, A. J.; Mohler, E. R., 3rd; Nicolau, J. C.; Pais, P.; Parkhomenko, A.; Pedersen, T. R.; Pella, D.; Ramos-Corrales, M. A.; Ruda, M.; Sereg, M.; Siddique, S.; Sinnaeve, P.; Smith, P.; Sritara, P.; Swart, H. P.; Sy, R. G.; Teramoto, T.; Tse, H. F.; Watson, D.; Weaver, W. D.; Weiss, R.; Viigimaa, M.; Vinereanu, D.; Zhu, J.; Cannon, C. P.; Wallentin, L. Darapladib for preventing ischemic events in stable coronary heart disease. *N. Engl. J. Med.* **2014,** *370*, 1702-1711; (b) O'Donoghue, M. L.; Braunwald, E.; White, H. D.; Lukas, M. A.; Tarka, E.; Steg, P. G.; Hochman, J. S.; Bode, C.; Maggioni, A. P.; Im, K.; Shannon, J. B.; Davies, R. Y.; Murphy, S. A.; Crugnale, S. E.; Wiviott, S. D.; Bonaca, M. P.; Watson, D. F.; Weaver, W. D.; Serruys, P. W.; Cannon, C. P.; Steen, D. L. Effect of darapladib on major coronary events after an acute coronary syndrome: the SOLID-TIMI 52 randomized clinical trial. *JAMA* **2014,** *312*, 1006-1015; (c) Yeo, A.; Li, L.; Warren, L.; Aponte, J.; Fraser, D.; King, K.; Johansson, K.; Barnes, A.; MacPhee, C.; Davies, R.; Chissoe, S.; Tarka, E.; O'Donoghue, M. L.; White, H. D.; Wallentin, L.; Waterworth, D. Pharmacogenetic meta-analysis of baseline risk factors,

pharmacodynamic, efficacy and tolerability endpoints from two large global cardiovascular outcomes trials for darapladib. *PLoS One* **2017,** *12*, e0182115.

17. Mullard, A. GSK's darapladib failures dim hopes for anti-inflammatory heart drugs. *Nat. Rev. Drug Discov.* **2014,** *13*, 481-482.

18. Staurenghi, G.; Ye, L.; Magee, M. H.; Danis, R. P.; Wurzelmann, J.; Adamson, P.; McLaughlin, M. M. Darapladib, a lipoprotein-associated phospholipase A2 inhibitor, in diabetic macular edema: a 3-month placebo-controlled study. *Ophthalmology* **2015,** *122*, 990-996.

19. Maher-Edwards, G.; De'Ath, J.; Barnett, C.; Lavrov, A.; Lockhart, A. A 24-week study to evaluate the effect of rilapladib on cognition and cerebrospinal fluid biomarkers of Alzheimer's disease. *Alzheimer's Dementia: Transl. Res. Clin. Interventions* **2015,** *1*, 131-140.

20. Chen, X.; Wang, K.; Xu, W.; Ma, Q.; Chen, M.; Du, L.; Mo, M.; Wang, Y.; Shen, J. Discovery of potent and orally active lipoprotein-associated phospholipase A2 (Lp-PLA2) inhibitors as a potential therapy for diabetic macular edema. *J. Med. Chem.* **2016,** *59*, 2674-2687.

21. Erlanson, D. A.; Fesik, S. W.; Hubbard, R. E.; Jahnke, W.; Jhoti, H. Twenty years on: the impact of fragments on drug discovery. *Nat. Rev. Drug Discov.* **2016,** *15*, 605-619.

22. Woolford, A. J.; Pero, J. E.; Aravapalli, S.; Berdini, V.; Coyle, J. E.; Day, P. J.; Dodson, A. M.; Grondin, P.; Holding, F. P.; Lee, L. Y.; Li, P.; Manas, E. S.; Marino, J., Jr.; Martin, A. C.; McCleland, B. W.; McMenamin, R. L.; Murray, C. W.; Neipp, C. E.; Page,

L. W.; Patel, V. K.; Potvain, F.; Rich, S.; Rivero, R. A.; Smith, K.; Somers, D. O.; Trottet, L.; Velagaleti, R.; Williams, G.; Xie, R. Exploitation of a novel binding pocket in human lipoprotein-associated phospholipase A2 (Lp-PLA2) discovered through X-ray fragment screening. *J. Med. Chem.* **2016,** *59*, 5356-5367.

23. Woolford, A. J.; Day, P. J.; Beneton, V.; Berdini, V.; Coyle, J. E.; Dudit, Y.; Grondin, P.; Huet, P.; Lee, L. Y.; Manas, E. S.; McMenamin, R. L.; Murray, C. W.; Page, L. W.; Patel, V. K.; Potvain, F.; Rich, S. J.; Sang, Y.; Somers, D. O.; Trottet, L.; Wan, Z.; Zhang, X. Fragment-based approach to the development of an orally bioavailable lactam inhibitor of lipoprotein-associated phospholipase A2 (Lp-PLA2). *J. Med. Chem.* **2016,** *59*, 10738-10749.

24. Hopkins, A.; L.Groom, C.; R.Alex, A. Ligand efficiency: a useful metric for lead selection. *Drug Discov. Today* **2004,** *9*, 430-431.

25. (a) Cao, J.; Hsu, Y. H.; Li, S.; Woods, V. L.; Dennis, E. A. Lipoprotein-associated phospholipase A(2) interacts with phospholipid vesicles via a surface-disposed hydrophobic alpha-helix. *Biochemistry* **2011,** *50*, 5314-5321; (b) Cao, J.; Hsu, Y. H.; Li, S.; Woods, V. L., Jr.; Dennis, E. A. Structural basis of specific interactions of Lp-PLA2 with HDL revealed by hydrogen deuterium exchange mass spectrometry. *J. Lipid Res.* **2013,** *54*, 127-133.

26. Six, D. A.; Dennis, E. A. The expanding superfamily of phospholipase A(2) enzymes: classification and characterization. *Biochim. Biophys. Acta* **2000,** *1488*, 1-19.

27. McGinnity, D. F.; Soars, M. G.; Urbanowicz, R. A.; Riley, R. J. Evaluation of fresh

and cryopreserved hepatocytes as in vitro drug metabolism tools for the prediction of metabolic clearance. *Drug Metab. Dispos.* **2004,** *32*, 1247-1253.

28. Nonlinear regression was performed using GraphPad Prism version 5.00 for Windows, GraphPad Software, San Diego California USA, www.graphpad.com.

29. Wang, Q. S.; Yu, F.; Huang, S.; Sun, B.; Zhang, K. H.; Liu, K.; Wang, Z. J.; Xu, C. Y.; Wang, S. S.; Yang, L. F.; Pan, Q. Y.; Li, L.; Zhou, H.; Cui, Y.; Xu, Q.; Earnest, T.; He, J. H. The macromolecular crystallography beamline of SSRF. *Nucl. Sci. Tech.* **2015,** *26*, 12-17.

30. Minor, W.; Cymborowski, M.; Otwinowski, Z.; Chruszcz, M. HKL-3000: the integration of data reduction and structure solution--from diffraction images to an initial model in minutes. *Acta Crystallogr. D Biol. Crystallogr.* **2006,** *62*, 859-866.

31. McCoy, A. J.; Grosse-Kunstleve, R. W.; Adams, P. D.; Winn, M. D.; Storoni, L. C.; Read, R. J. Phaser crystallographic software. *J. Appl. Crystallogr.* **2007,** *40*, 658-674.

32. Adams, P. D.; Afonine, P. V.; Bunkoczi, G.; Chen, V. B.; Davis, I. W.; Echols, N.; Headd, J. J.; Hung, L. W.; Kapral, G. J.; Grosse-Kunstleve, R. W.; McCoy, A. J.; Moriarty, N. W.; Oeffner, R.; Read, R. J.; Richardson, D. C.; Richardson, J. S.; Terwilliger, T. C.; Zwart, P. H. PHENIX: a comprehensive Python-based system for macromolecular structure solution. *Acta Crystallogr. D Biol. Crystallogr.* **2010,** *66*, 213-221.

33. Emsley, P.; Lohkamp, B.; Scott, W. G.; Cowtan, K. Features and development of Coot. *Acta Crystallogr. D Biol. Crystallogr.* **2010,** *66*, 486-501.

34. (a) Berry, M. N.; Friend, D. S. High-yield preparation of isolated rat liver

parenchymal cells: a biochemical and fine structural study. *J. Cell Biol.* **1969,** *43*, 506-520; (b) Orrenius, S.; Thor, H.; Rajs, J.; Berggren, M. Isolated rat hepatocytes as an experimental tool in the study of cell injury. Effect of anoxia. *Forensic Sci.* **1976,** *8*, 255-263.

Table of contents graphic